Photogenerated Charge Transport in Organic Electronic Materials: Experiments Confirmed by Simulations

Armantas Melianas and Martijn Kemerink

Melianas, A., Kemerink, M., (2019), Photogenerated Charge Transport in Organic Electronic Materials: Experiments Confirmed by Simulations, *Advanced Materials*, 31(22), 1806004.
https://doi.org/10.1002/adma.201806004

DOI: 10.1002/ ((please add manuscript number))
Article type: Progress Report

Photogenerated Charge Transport in Organic Electronic Materials: Experiments Confirmed by Simulations

Armantas Melianas[*]*, Martijn Kemerink*[*]

This publication is dedicated to Olle Inganäs on the occasion of his retirement. Many of the ideas presented in this work came forward in discussions with Olle and this Progress Report offers a glimpse into his and our combined thought process. We are grateful for his inspiration and critical input.

Dr. Armantas Melianas
Department of Materials Science and Engineering, Stanford University, Stanford, California 94305, USA
E-mail: armantas.melianas@stanford.edu

Prof. Martijn Kemerink
Complex Materials and Devices, Department of Physics, Chemistry and Biology, Linköping University, 58183 Linköping, Sweden
E-mail: martijn.kemerink@liu.se

Keywords: thermalization, organic solar cells, kinetic Monte Carlo simulations, charge carrier mobility, non-equilibrium phenomena

Abstract

The performance of organic optoelectronic devices, such as organic photovoltaic (OPV) cells, is to a large extent dictated by their ability to transport the photogenerated charge, with relevant processes spanning a wide temporal (fs-µs) and spatial (1-100 nm) range. However, time-resolved techniques can access only a limited temporal window, and often contradict steady-state measurements. In this progress report, we unify commonly employed steady-state and time-resolved techniques over an exceptionally wide temporal range (fs-µs) in a consistent physical picture. We show experimental evidence confirmed by numerical simulations that, although various techniques probe different time scales, they are mutually consistent as they probe the same physical mechanisms governing charge motion in disordered media – carrier hopping and thermalization in a disorder-broadened density of states (DOS). We highlight the

generality of this framework by time-resolved experimental data obtained on polymer:fullerene, polymer:polymer and small molecule blends with varying morphology, including recent experiments revealing that low donor content OPV devices operate by long-range hole tunneling between non-nearest-neighbor molecules. This progress report reviews the importance of non-equilibrium processes in organic electronic materials, with a particular focus on experimental data and understanding charge transport physics in terms of material DOS.

1. Introduction

Organic semiconductors show great promise for use in low-cost optoelectronic devices, such as organic photovoltaic (OPV) devices[1–4] and photodetectors.[5] In these devices, the photoactive layer typically consists of a disordered bulk heterojunction (BHJ) mixture of an electron donor (D) and an electron acceptor (A). Following photoexcitation, the relevant processes taking place in the BHJ mixture, such as charge generation, transport to the electrodes and recombination occur over a wide range of time (fs-µs) and length (1-100 nm) scales. All of these processes are dictated by the motion of photogenerated charges, which is related to the charge carrier mobility.

Although various time-resolved and steady-state techniques[6–15] are available to probe the charge carrier mobility in OPVs they often lead to different mobility values, even for one and the same material system. **Figure 1**a shows the trend in typical photogenerated carrier mobility values measured in various OPV systems.[6,8,11,16–30] Despite such large differences in mobility estimates, it is often assumed that charge carrier mobility in OPV devices can be determined by a single experimental technique, yielding a well-defined mobility. In this progress report, we challenge this notion by summarizing recent time-resolved experimental data confirmed by three dimensional (3D) kinetic Monte Carlo (kMC) simulations over an exceptionally wide temporal range (fs-µs) in a consistent physical picture. We emphasize that charge motion in OPV devices is dominated by transient (i.e. non-equilibrium) effects, which cannot be revealed

by a single experimental technique – to fully understand photogenerated charge transport in organic electronic materials, all relevant time scales must be accounted for.

We place particular emphasis on experiments and simulations enabling us to visualize the energetic position of the photogenerated carriers in their respective DOS, which is critically related by thermodynamics to the maximum attainable open-circuit voltage (V_{OC}) and thus the power conversion efficiency (PCE) of any photovoltaic device.[31,32] From a practical standpoint, this approach is motivated by the fact that although state-of-the-art OPV devices are reasonably efficient in terms of light in-coupling and photocurrent generation (peak external quantum efficiency (EQE) values of ~80 % over the absorbing range are attainable[1]), they are still relatively poor in utilizing the absorbed photon energy. V_{OC} losses, defined as the difference between the optical gap (E_{opt}) and the open-circuit voltage (V_{OC}), for OPVs are typically >0.5 eV, considerably larger than for other, for instance inorganic or perovskite, solar cell technologies.[33] These losses occur gradually, following the absorption of photons, with different processes occurring at different time scales, which are at least in part accessible by time-resolved measurements.

Although in this progress report we illustrate the main charge transport ideas using time-resolved experimental data taken on OPV devices based on D/A organic semiconductor blends, the results are expected to be equally applicable to any organic semiconductor due to the generality of the employed formalism. We rely on the Gaussian Disorder Model (GDM),[24,34,35] which has been successfully utilized to explain charge transport in a large variety of organic semiconductors in the past. As such, this progress report reviews the general importance of non-equilibrium processes in organic electronic materials, with a particular focus on experimental data and understanding charge transport physics in terms of material DOS.

2. Non-equilibrium motion of photogenerated charges

Here we discuss the starting position of the photogenerated charges in their respective DOS following photoinduced electron (or hole) transfer (Figure 1b), and their fate at longer time scales relevant for charge transport. Following photoinduced charge generation, the excess photon energy is temporarily stored in the non-equilibrated photogenerated charge population. This affects charge motion until full equilibration (i.e. excess photon energy dissipation by thermalization) takes place (Figure 1b). As we will show below, in disordered materials, such as organic semiconductors, photogenerated charges can be transported over substantial distances before full thermalization takes place.[20,21]

In optimized OPV systems the initial photo-induced electron (or hole) transfer from the lowest unoccupied molecular orbital (LUMO) of the donor to the LUMO of the acceptor is known to occur in ~1 ps or less.[36,37] The distribution of available LUMO DOS sites for electron transfer (and at later time scales for charge transport) are broadened by, typically Gaussian, disorder, as schematically illustrated in Figure 1b. Statistically speaking, upon absorption in a Gaussian DOS, the electron-hole pair is most likely created in the center of their respective DOS as most sites are available at that energy (Figure 1b). Regardless of the initial electron energy in the donor LUMO manifold, and thus regardless of the photon energy, the electron is statistically most likely to transfer to the center of the acceptor LUMO DOS (or to the highest occupied molecular orbital (HOMO) DOS for hole transfer). As a consequence, at short time scales following electron-hole pair generation, both the photogenerated electron and hole are situated at relatively high energy sites in their respective DOS high (i.e. close to the Gaussian DOS center in Figure 1b). Although these qualitative rules might be expected to no longer hold for photoexcitation in the charge transfer (CT) manifold, we will show below that even under such conditions photogenerated carrier thermalization phenomena are prominently present (Section 7.1).

Since there are many DOS sites at lower energies, the excess photon energy may be expected to quickly dissipate as heat by a step-wise release of phonons. In other words, the photogenerated charges are expected to thermalize to their DOS quasi-equilibrium energies before any significant charge transport has occurred. Following this ultrafast (e.g. ~1 ps) thermalization, the photogenerated carriers are then transported to the electrodes at their DOS quasi-equilibrium energies. In this scenario, charge transport can be described by a well-defined mobility. While these assumptions are experimentally justified for conventional inorganic semiconductors (without localized traps extending into the bandgap), for example in crystalline Si photogenerated carrier thermalization completes in less than ~1 ps,[38,39] rapid thermalization is generally not the case for disordered materials,[40–42] such as organic semiconductors. The reason is that sites at lower energies become increasingly sparse, and that, to relax to deeper sites, charges increasingly need to be excited from their present site.[43] Nevertheless, despite lack of experimental proof, assumptions of rapid thermalization, quasi-equilibrium and well-defined mobilities are still widespread in the OPV community. Here we emphasize that these notions are inconsistent with experimental results.

In fact, previous experimental and theoretical studies show strong indications that photogenerated carrier thermalization in organic semiconductors is relatively slow.[8,11,24,25] Furthermore, reported charge carrier mobility values typically differ by orders of magnitude when probed at different time scales following photoexcitation (Figure 1a). Slow thermalization is well-known from past literature describing photogenerated charge transport in disordered inorganic semiconductors, for instance amorphous inorganic solar cells, containing a strongly energy-dependent distribution of localized trap sites inside the bandgap.[40–42] Theoretically, thermalization in a strongly decaying DOS tail is expected to occur over (exponentially) extended time scales, similar as shown in Figure 1c. Since charge transport in organic semiconductors also takes place in a broad distribution of localized sites (due to weak intermolecular coupling and large disorder), photogenerated carrier thermalization should

therefore also occur gradually, over time scales much longer than ~1 ps. The gradual trapping of the photogenerated carriers to lower lying localized sites generally leads to a time-dependent carrier mobility, which decreases with time following photoexcitation, similar to the mobility data trend in Figure 1a.

Carrier thermalization in disordered organic solids has been extensively studied in the past, initially by time-of-flight (TOF) mobility measurements.[24] Arguably the most successful theoretical model, rationalizing those findings, was developed by Bässler and coworkers.[24] The model describes charge motion in a Gaussian distribution of localized sites (section 2.1) and can predict the dynamics of carrier thermalization (Figure 1c). However, due to the limited temporal resolution of TOF measurements (typically >100 ns), the model predictions were initially difficult to quantitatively confirm over the full range of relevant time scales (fs-μs).

The development of new experimental techniques has extended the accessible temporal range quite significantly. For example, Figure 1a shows typical carrier mobility values found in various OPV systems,[6,8,11,16–30] as estimated by the indicated experimental technique: Time-resolved Electro-Absorption (EA), Time-Resolved Terahertz Spectroscopy (TRTS), Time-Resolved Electric-Field-Induced Second-Harmonic generation (TREFISH), Time-Resolved Microwave Conductance (TRMC), Photogenerated Charge Extraction by Linearly Increasing Voltage (pCELIV), transient photocurrent or time-of-flight (TOF) and Space-Charge-Limited-Currents (SCLC).

The trend in the mobility data (Figure 1a) strongly resembles the gradual thermalization of photogenerated charges as predicted by theory (Figure 1c), suggesting that the two phenomena are coupled – photogenerated carrier thermalization is driven by charge motion and leads to a time-dependent mobility. This observation casts doubt on the often-implicit notion that carrier thermalization in organic semiconductors is incredibly fast. Although most researchers in the field are well aware of this and would agree that photogenerated charge motion in organic semiconductors should be described as a non-equilibrium transient process, the assumptions of

rapid thermalization, quasi-equilibrium and well-defined carrier mobilities remain widespread in the OPV community, as reflected by for example the use of drift-diffusion device models and steady-state mobilities. Transient charge transport measurements are typically discussed in isolation and kept far from quantitative device modeling. This oversight possibly originates from a lack of comprehensive experimental studies and an accompanying framework that is able to explain all relevant time scales. This progress report is an attempt to outline such a framework.

Here, we unify commonly used time-resolved techniques and simulations over an exceptionally wide temporal range (fs-µs and steady-state) in a consistent physical picture to show that, although they probe different time scales, they are mutually consistent as they probe the same physical mechanism governing charge motion – carrier hopping and thermalization in a disorder broadened density of states (Figure 1). Since carrier thermalization occurs downhill in energy, we show that carrier motion is boosted by this process, leading to a time-dependent carrier mobility (Figure 1a). We confirm this picture by a combination of very different transient techniques shown in Figure 1a: TRTS, TREFISH, TRMC combined with Transient Absorption (TA) measurements, pCELIV, transient photocurrent and TOF; and describe the relation of these transient techniques to steady-state mobility measurements in the dark (i.e. without photoexcitation), such as SCLC (Figure 1a). In this description, the difference between steady-state and ultrafast time-resolved techniques follows naturally, since they probe the motion of charges residing at different energies in the DOS. Furthermore, we discuss how non-equilibrium charge motion affects charge carrier separation and recombination dynamics, and present an outlook on how these processes could affect OPV device performance, particularly device V_{OC}. We highlight the generality of our framework by time-resolved experimental data obtained on polymer:fullerene[19–21,44,45], polymer:polymer[20] and small molecule blends with varying morphology,[22] including recent experiments on OPV systems with low donor content revealing that they operate on basis of long-range hole tunneling between non-nearest-neighbor

molecules.[22] We identify the time and distance scales relevant for charge extraction to show that experimental techniques that probe the mobility of (almost) thermalized charge carriers are not necessarily meaningful to OPV device operation. There is no unique mobility[19] – the mobility of photogenerated charges is, in most cases, time-dependent, as it gradually decreases following photoexcitation.[21] In addition, we show that the mean mobility at any point in time is also a poor measure of the motion of the ensemble of photogenerated charges, since not all charges behave identically.[19] Therefore, for a full description of organic semiconductors, non-equilibrium effects related to the gradual thermalization of the photogenerated carrier populations, as probed by ultra-fast time-resolved techniques, must be accounted for.

2.1. Brief introduction to the Gaussian Disorder Model (GDM)

This section is intended as a brief introduction to the Gaussian Disorder Model (GDM),[24,34] highlighting its main features and assumptions, particularly in the context of modelling time-resolved experiments using 3D kMC simulations. In our own work, we have found that GDM can successfully describe a large number of transient experiments, spanning a wide range of times, using the least number of parameters, most of which can be determined from experiments.[19–23,44,45] Nevertheless, such generality comes at a cost of losing morphology specific information (such as the interplay between ordered and disordered regions of the semiconducting film), which is particularly relevant when describing ultrafast time scales, but not the main purpose of this progress report. The influence of sample morphology on photogenerated charge transport is addressed in section 7. Although here the GDM concepts are illustrated for a polymer film, the same reasoning is applicable to small molecule films or mixtures of polymers and/or small molecules.

The GDM model describes charge motion in an energetically disordered landscape, for example hole transport in the polymer donor phase (**Figure 2**a). Chemical and physical defects, chain kinks and chain ends break the polymer chain into subunits or conjugated units, which serve as

electronic sites for charge transport (Figure 2b). Due to disorder, the wavefunctions at each site are strongly localized, as first elucidated by Anderson.[46] This is the origin of low conductivity in organic semiconductors. Nevertheless, charge transport between localized sites can occur by thermally activated tunneling, commonly referred to as hopping (Figure 2c and 2d). The hopping rate from an initial state *i* with energy E_i to a final state *f* with energy E_f can be described with the least number of unknown parameters by the Miller-Abrahams expression,[47] which relies on a phonon-assisted tunneling mechanism

$$\nu_{if} = \begin{cases} \nu_0 \exp(-2\alpha r_{if}) \exp\left(-\frac{E_f - E_i}{kT}\right) & \text{if } \Delta E_{if} = E_f - E_i > 0 \\ \nu_0 \exp(-2\alpha r_{if}) & \text{if } \Delta E_{if} = E_f - E_i \leq 0 \end{cases} \quad (1)$$

where ν_0 is the carrier attempt-to-hop frequency, generally understood to be related to some phonon frequency in the material, r_{if} is the distance between localized sites, *k* is the Boltzmann constant, *T* is the temperature. To account for an externally applied electric field or Coulomb interaction with nearby charges, the site energies in the second exponent must be corrected for the resulting electrostatic energy terms. The parameter α describes the decay length of the localized wavefunctions. Typically, α^{-1} ~0.1 nm is used, meaning that the charge carriers are strongly localized on a single site and that only nearest-neighbor hopping is possible. This assumption relies on experimentally determined values for TNF:PVK (α^{-1} ~0.11 nm)[48] and for P3HT and OC_1C_{10}-PPV (α^{-1} ~0.15 nm)[49] (full material names are provided at the end of this publication). By analyzing temperature-dependent SCLC data we recently found α^{-1} ~0.25 nm for a range of pure materials and blends.[50] However, using OPV blends with low donor content, we have shown that α^{-1} ~1 nm is also possible,[22] facilitating long-range hopping between non-nearest-neighbor molecules (section 7.2).

In our own work, we have found that to successfully fit time-resolved experimental data over a wide temporal range (fs-µs), it is not strictly necessary to explicitly account for the inter-site distance dependence. More concretely, we have integrated the first exponential in Equation (1)

into a material-specific constant v_0. In addition, since placing a charge on a molecular site deforms the molecule and its environment (i.e. creates a polaron), Marcus theory[51] may appear more suitable to describe the hopping rate, replacing Equation (1). Nevertheless, we have thus far been able to successfully model time-resolved experimental data using the simplified version of the Miller-Abrahams rate, not accounting for the inter-site distance dependence and not accounting for polaronic effects. On occasions we have compared the different rates and found no experimentally relevant differences in the resulting non-equilibrium charge transport behavior.

The energy distribution of localized sites through which hopping takes place is assumed to be Gaussian

$$(E_\mathrm{i}) = \frac{1}{\sqrt{2\pi\sigma^2}} \exp\left(-\frac{(E_\mathrm{i}-E_0)^2}{2\sigma^2}\right) \quad (2)$$

where E_i is the single particle energy on site i, E_0 is the mean energy and σ is the standard deviation of the Gaussian DOS or simply the energetic disorder. An exponential DOS may be used instead, however, for the OPV materials we have experimentally investigated thus far, including polymer:fullerene,[19–21,44,45] polymer:polymer[20] and small molecule blends with varying morphology,[22] the Gaussian DOS was found to fit the experimental data best. In addition, an exponential DOS predicts that carrier thermalization proceeds indefinitely, without stopping at quasi-equilibrium DOS energies,[43] which is inconsistent with experiments. The D/A materials discussed in this progress report span the energetic disorder range σ = 60-140 meV, which is typical for organic semiconductors.[49,50]

The spatial arrangement of the polymer chains (i.e. film morphology), determines the spatial distribution of the electronic sites. Unfortunately, such spatial distributions are not directly accessible by experiments. Hence, the GDM model relies on two further simplifications. First, the electronic sites are represented as a grid with an effective inter-site distance a_nn (Figure 2c), typically in the range of a_nn = 0.3-2 nm.[52] This approach has worked remarkably well for a

large number of organic semiconductors. On basis of earlier work[44,45] where experiments were fitted by the GDM, we typically use a_{nn} = 1.8 nm, a choice that was further confirmed by analysis of temperature-dependent SCLC experiments on pristine materials and blends.[50] Second, the photoactive film is treated as an effective medium, meaning that the nanoscale morphology of the BHJ film is not explicitly accounted for. In this case, the used HOMO and LUMO levels correspond to hole transport in the donor (HOMO) and electron transport in the acceptor (LUMO) materials of the BHJ blend, respectively.

Although amorphous OPV films may have nanoscale morphological variations, for example fullerene domains that are too small to resolve using microstructural characterization tools, the effective medium approximation remains valid. In any morphology, thermalization begins in the phase where the charge carrier is initially photogenerated and transported, for example in an amorphous region, followed by charge transport and thermalization in a more ordered region, since ordered regions are lower in energy. The extent of thermalization in each phase is set by its energetic disorder and the fraction of time the photogenerated carrier resides in each phase. Even in the case of complex morphologies, the use of an effective medium approximation can describe some average of the full thermalization kinetics.

Nevertheless, by mapping the multi-length scale morphology of the polymer film on a grid, morphology-specific information as well as the effects of spatial disorder are to a large extent lost. Hence, the GDM parameters, such as the inter-site distance a_{nn}, the attempt-to-hop frequency ν_0 and the energetic disorder σ, represent average or effective values over the entire film. This approximation is most suitable for amorphous polymer films without complex hierarchical morphology involving amorphous, semi-crystalline and crystalline regions. Although the model conclusions are general and expected to apply to any morphology (but with added complexity), to illustrate the main concepts, we first focus on well inter-mixed and amorphous OPV blends, such as TQ1:$PC_{71}BM$ (1:2.5)[53] and PCDTBT:$PC_{61}BM$ (1:2)[54] (D:A

ratios throughout this publication refer to weight ratio unless otherwise noted), and will cover more complex morphologies in section 7.

Some of the limitations of lattice models can be taken away by analytical treatments. In particular, multiple-trapping (or equivalently mobility edge) models can be used to describe the bare charge carrier thermalization behavior in exponential or Gaussian DOS.[40–42] Recently, Hofacker et al. extended the "demarcation energy" concept to describe the dispersive recombination of photogenerated charges in disordered organic semiconductors[55,56] that results from the decay in carrier mobility that accompanies thermalization. In ref. [57] we reported a first attempt to integrate the multiple trapping concept in a full OPV device model including dispersive transport and Ohmic contacts; the time gain compared to 3D kMC allowed the least-squares fittings shown in section 7.1. In section 4.1 we shall touch upon other kinetic aspects of carrier recombination that require a quasi-atomistic description like kinetic Monte Carlo.

As a final note, we point out that the GDM model is a crude description of ultrafast, and in literature suggested to be coherent,[37,58] phenomena occurring on femtosecond to picosecond time scales. In addition, charge transport at the shortest time scales is expected to take place along the polymer backbone,[27] which is not explicitly accounted for by the GDM model (the polymer chain is reduced to grid-like sites, see Figure 2). Models incorporating the spatial arrangement of the polymer chains have been proposed.[59] Although GDM is a rough approximation of the phenomena occurring at the earliest time and shortest length scales, it is important to realize that the main purpose of the model is not to fit a limited temporal range. The main purpose of the model is to use a single framework that describes a large number of transient experiments, spanning a wide range of times (fs-μs), and to accomplish this by the least number of parameters, most of which can be determined from experiments.

2.2. Photogenerated carrier thermalization according to the GDM framework

Within the framework of the GDM model, photogenerated carrier thermalization can only take place by hopping motion between localized sites. Since on-site carrier thermalization is expected to occur very fast <1 ps,[60,61] for the time scales investigated here, it can be considered instantaneous. We further consider only inter-site thermalization by hopping motion (Figure 1 and 2).

According to the Miller-Abrahams expression Equation (1), hops that are downward in energy ($\Delta E_{if} < 0$), such as during the initial stages of carrier thermalization, occur at a considerably higher rate than upward hops. This is because downward hops are not subject to the Boltzmann factor that reduces the hopping rate for upward hops ($\Delta E_{if} > 0$). As a consequence, a charge carrier initially positioned at an energy E_0 will rapidly thermalize to lower energy sites and eventually to its quasi-equilibrium energy, which is $-\sigma^2/kT$ away (in the Boltzmann limit of low carrier density) from the Gaussian DOS center. We have shown that for sufficiently thin films (~100 nm) the photogenerated carriers can be extracted from the OPV device before full thermalization takes place (Figure 1b).[21]

Using a combination of time-resolved measurements and 3D kMC simulations we have also shown that photogenerated carrier thermalization in disordered organic semiconductors is a two-step process (Figure 1b).[21] At early time scales (~1–100 ns) a substantial amount of energy (~1-2σ) is dissipated by fast diffusive motion (red in Figure 1b), during which most of the hops occur downward in energy and are therefore insensitive to electric field F (i.e. drift).[21] Time-resolved electric-field-induced second harmonic generation (TREFISH) measurements performed by other groups corroborate this observation, showing that the initial charge separation processes on picosecond to nanosecond time scales is indeed driven by diffusion in an energetically disordered medium.[62] In addition, earlier TREFISH measurements performed on neat polymer films have confirmed that initial thermalization is temperature-independent.[63] This was rationalized by the GDM model, where carrier hopping, following the earliest time

scales after photoexcitation, occurs downward in energy and does not require thermal activation. The diffusion part of the energy loss to thermalization can be minimized only by reducing the energetic disorder of the material.

In contrast, at later time scales, an increasing number of upward hops is required for long-range motion and thermalization slows down considerably (blue in Figure 1b). This observation is supported by earlier TREFISH measurements on neat polymer films, showing that at longer time scales following photoexcitation charge carrier motion becomes temperature-dependent.[63] During charge drift to the electrodes, the remaining excess photon energy is further dissipated as heat. For an optimized ~70 nm thick TQ1:$PC_{71}BM$ (1:2.5) device, we have estimated an additional loss of ~0.5-1σ during charge drift to the extracting electrodes (Figure 1b blue arrows) at short-circuit and maximum power point (MPP) conditions, respectively, and found that the photogenerated carriers are extracted before reaching quasi-equilibrium at σ^2/kT below the center of their DOS (dotted line in Figure 1b).[21] Generally speaking, when using sufficiently thin OPV films (~100 nm) the photogenerated carriers can be extracted before thermalization completes.[21] In this case, reducing the energetic disorder would minimize the energy losses to thermalization, as would the use of thinner OPV layers.

3. Sample geometry and optical path considerations for time-resolved experiments

Before discussing experimental data, we point out several aspects regarding sample choice and preparation, which are important when analyzing experimental data. Time-resolved experiments probing the dynamics of photoexcited species in organic electronic materials are typically performed either on films coated on transparent insulating substrates, or on complete devices, for example films with electrodes (**Figure 3**). In most cases, an optical pump beam is absorbed by the film and creates photoexcited species. The dynamics of these species and the

altered properties of the OPV film are subsequently monitored by a time-delayed optical probe beam, with the temporal range set by the signal-to-noise ratio in the detected optical probe.

Transient measurements on complete devices (e.g. films with electrodes), are preferable. This is mostly because transient data can then be directly compared to steady-state device characteristics on the same device, allowing to check whether transient data represents the conditions relevant for steady-state device operation. In addition, the presence of electrodes may (or may not) alter the dynamics of the photoexcited species in the film. By measuring complete devices, effects due to the presence of the electrodes are, at least in part, included in the monitored dynamics. Electrodes also allow for bias-dependent measurements and for the detection of time-resolved electrical signals (in one shot, i.e. using the same pump pulse), such as transient photocurrent, pCELIV or TOF, providing complementary information to optical probing.[8,64]

However, OPV devices generally have only one semi-transparent electrode that allows for the light to enter. After traversing the OPV film the probe beam is reflected at the metallic contact and can be collected by a detector in "reflection mode". Although this is a common measurement geometry, it is fairly limited in the sense that the OPV device can only be photoexcited and probed from the same side. Thin film interference effects, resulting in spatially inhomogeneous charge generation and probe profiles, must also be accounted for.[65] As an alternative, semi-transparent OPV devices, where both electrodes are semi-transparent,[66] can be employed instead, enabling one to change the side at which the photoexcitation or the probe beam are incident on the OPV device, and significantly diminishing thin film interference effects.[19] In ref. [19], by probing the OPV device from different directions, we were able to independently measure the electron and hole transients with optical (i.e. sub-picosecond) temporal resolution in a complete OPV device (Figure 3c). The experiment is briefly described in the Figure 3c caption, more details can be found in refs. [19,23].

Measurements on complete OPV devices are not always possible. For example, TRTS and TRMC measurements require insulating substrates, typically quartz. In this case the optical probe is detected in "transmission mode" after traversing the OPV film (Figure 3a). The advantage of not having electrodes is ease of sample preparation – the OPV film is simply coated on a suitable pre-cleaned substrate. However, coating the film on quartz (or glass), does not necessarily guarantee the same OPV film morphology as in the corresponding OPV device. A different surface energy of quartz (or glass) compared to the substrate used for OPV device preparation can unintentionally result in a different OPV film morphology. This issue can be resolved by coating a suitably chosen interface material (e.g. a monolayer) prior to active layer deposition, both during OPV device fabrication and when OPV films are prepared on quartz (or glass) substrates. We have employed this strategy in our own work to ensure reliable comparison between transient data collected on films with and without electrodes.[21]

4. Photogenerated carrier thermalization

To experimentally probe photogenerated carrier thermalization in their respective DOS following photoexcitation we use Transient Absorption (TA) measurements using broadband (i.e. white light supercontinuum) probe pulses (**Figure 4**a and 4b). Using TA, the spectral dynamics of photoexcited species can be monitored over a wide temporal range (100 fs – 10 μs) in thin films or complete OPV devices. We rely on the fact that the broadening and the energetic position of the observed spectral features are related to DOS energetic disorder. This can be used to estimate the energetic position of the photogenerated carriers in their respective DOS, as outlined below.

Following photoexcitation ($t = 0$), a fraction of the molecules (or chromophores in the polymer) are promoted to an excited state, decreasing the fraction of molecules in the ground state. Since ground state absorption of the photoexcited sample is less than in the non-excited sample, the change in sample transmission ΔT relative to the non-excited sample transmission T is positive

($\Delta T/T > 0$); this is referred to as the Ground State Bleach (GSB), see Figure 4. In addition, the photoexcited species (e.g. holes on the polymer) generally also contribute to the TA spectrum via allowed optical transitions to higher excited states, resulting in Photoinduced Absorption (PIA, $\Delta T/T < 0$). In polymer:fullerene blends (discussed in this section) these optical signatures are typically dominated by optical signatures originating from the donor polymer. Since the GSB feature is due to the presence of a hole polaron on the polymer, the spectral position of the GSB peak maximum is indicative of the hole energetic position in the HOMO DOS. Hence, temporal redshifts of the GSB peak maximum can be utilized as a measure for hole thermalization. To the best of our knowledge, there is no technique that can monitor the thermalization of photogenerated electrons in fullerenes since the optical signatures originating from fullerenes are significantly weaker. The PIA band is routinely used as a measure for the hole polaron density, for example to study carrier recombination. We first discuss hole thermalization, the influence of thermalization to carrier recombination dynamics is discussed in section 4.1.

Figure 4 shows the gradual GSB redshift in TQ1:$PC_{71}BM$ (1:2.5)[21] and PCDTBT:$PC_{61}BM$ (1:2)[45], corresponding to a total redshift of ~100 meV and ~200 meV, respectively, which we have previously attributed to photogenerated hole thermalization[21] following the reasoning above. Most importantly, these experiments reveal that photogenerated carrier thermalization in organic semiconductors is gradual and can take as long as microseconds to complete (Figure 4a and 4b). In addition, we have previously shown using 3D kMC simulations that the factor ~2 difference in hole thermalization losses between the blends in Figure 4a and 4b stems from the difference in their HOMO DOS disorder values – PCDTBT:$PC_{61}BM$ (1:2) is considerably more disordered.[21,54] As a general rule, lower DOS energetic disorder leads to lower losses to thermalization. The implications of the above for the large V_{OC} losses typical for OPV[33] are currently unknown, see the Outlook section for further discussion.

The non-equilibrium nature of these processes is further corroborated by pump-fluence dependent TA measurements. Figure 3c shows that the GSB redshift in PCDTBT:$PC_{61}BM$ (1:2) is pump-fluence independent (i.e. initial carrier density independent), highlighting the non-equilibrium nature of the monitored dynamics.[45] This is also the case for TQ1:$PC_{71}BM$ (1:2.5).[21] In contrast, it is well known that at quasi-equilibrium such carrier density variations would have led to significant state-filling effects.[52,67] These experiments can be rationalized in the GDM framework, where considerably more transport sites are available at higher DOS energies, significantly diminishing carrier concentration effects. As such, pump-fluence independence of the GSB redshift dynamics originates from the non-equilibrium nature of photogenerated carrier thermalization as rationalized by the GDM.

As a final note, when employing these measurements, it is important to ensure that the PIA band does not induce an apparent temporal redshift of the GSB, which could occur if the two bands overlap in energy. We have carefully checked this not to be the case for the blends in Figure 4. However, this is not always the case. Despite these complications, to the best of our knowledge, the TA technique remains the most direct measure of hole thermalization dynamics in polymer:fullerene blends. Measurements on other OPV systems, particularly involving non-fullerene acceptors, would be highly interesting to confirm (or disprove) the validity and generality of the outlined approach.

4.1. Non-equilibrium charge separation and recombination

Since photogenerated carrier thermalization spans the temporal range relevant for charge separation, i.e. the spatial separation of the electron-hole pair following charge transfer (typically occurring at <1 ns time scales), and recombination (typically occurring at >1 ns time scales), it is unavoidable that these processes are affected by thermalization, and therefore by the underlying energetic disorder. In this section we discuss how these processes are affected by thermalization.

An in-depth discussion of charge separation mechanisms in OPV is, in view of the extensive and ongoing debate on this topic, beyond the scope of the present work, but we would like to point out that many of the proposed mechanisms, including interfacial dipoles,[68,69] entropic effects[69,70] and delocalization,[37,58,71–73] are of relatively short range (i.e. up to several nm). Due to the long-range nature of the Coulomb interaction it is, however, not evident that the correspondingly reduced electron-hole binding energy is easily overcome. For an average 4 nm electron-hole separation and a typical dielectric constant $\varepsilon_r = 3.6$, the Coulomb energy is ~0.1 eV, corresponding to ~4 kT at room temperature. Likewise, the electric field between the electron-hole pair at this distance is ~2.5×10^7 V/m, more than an order of magnitude larger than the effective field in a typical OPV device at MPP conditions. Hence, if long-range charge separation were an equilibrium process, the chances of escaping the Coulomb force would be very low, even in the presence of highly effective short-range separation mechanisms.

In 1995 Albrecht and Bässler used kMC to show that energetic disorder significantly enhances the probability of the electron-hole pair escaping from their mutual Coulomb attraction.[74] The key insight is that energy loss by thermalization in a broadened DOS counteracts energy gain by climbing up the Coulomb potential well. In later works, this concept has been refined by various authors, including a heterojunction interface,[75] experimentally determined GDM hopping parameters[44] and entropy effects.[76] In ref. [44] it was moreover shown that it is in principle possible to design a D/A heterojunction interface where energy losses and gains largely cancel while still giving rise to efficient charge separation. This prediction may have already been realized in non-fullerene bulk heterojunctions with low driving force, reducing voltage losses.[77]

The gradual thermalization of photogenerated charges also affects the carrier recombination dynamics. The bottom panel in Figure 4c shows that the integrated-intensity temporal dynamics of the GSB and PIA bands overlap, meaning that for PCDTBT:$PC_{61}BM$ (1:2) both bands originate from the same charge population (hole polaron). Further comparison of the top and

bottom panels of Figure 4c reveals that thermalization starts at ~200 ps, whereas charge recombination begins only when the photogenerated charges have almost fully thermalized at ~2 ns. By fitting the experimental data using 3D kMC simulations we have previously rationalized these findings: while the photogenerated holes and electrons residing at higher DOS energies often meet and form CT complexes, they do not recombine (Figure 4d).[45]

In fact, as we will demonstrate experimentally in section 5, photogenerated charge motion is boosted by thermalization (leading to a higher carrier mobility at early time scales[21,45]), enabling the photogenerated charges to repeatedly separate without recombination while they reside at higher DOS energies (Figure 4d). The idea that photogenerated charges repeatedly separate on picosecond time scales was earlier independently suggested on basis of kMC simulations by McGehee et al.[78]. Using TRMC and pCELIV experiments we have previously shown that at later ~10ns-µs time scales the photogenerated charges encounter/dissociate at a fixed rate,[29] whereas in a later publication we have suggested that, to explain the TA recombination dynamics in TQ1:$PC_{71}BM$ (1:2.5), a time-dependent photogenerated carrier mobility must be used.[64] As a consequence, only almost fully thermalized charges are expected to undergo recombination, as sketched in Figure 4d. In section 5 we will use independent experiments to confirm that these processes can indeed be rationalized by a time-dependent photogenerated carrier mobility.

5. Non-equilibrium charge extraction

In the previous section we have experimentally shown that photogenerated carrier thermalization can take as long as microseconds to complete.[21] Since photogenerated carrier extraction spans a similarly broad temporal range (fs-µs), it is expected that photogenerated carrier thermalization also affects charge motion. In this section, we describe time-resolved charge extraction measurements on complete OPV devices that monitor photogenerated carrier

dynamics over an exceptionally broad temporal range (100 fs – 10 μs), i.e. from photogeneration to full extraction. We elucidate the coupling between carrier thermalization and charge motion in the framework of GDM, corroborating the notion that only mostly fully thermalized charges undergo recombination (Figure 4c and d).

To fully understand charge transport, the motion of photogenerated charges must be experimentally measured at all relevant time scales – from the first hopping events to full extraction (~100 fs – 10 μs). Although photogenerated charge transport in OPV devices can be studied by means of transient photocurrent measurements, RC limitations generally limit their use to time scales longer than nanoseconds.[10,79] In contrast, the first hopping events occur on sub-picosecond to picosecond time scales. RC limitations can be avoided if the early time scales of charge motion are instead monitored by an optical probe.

5.1. TREFISH combined with transient photocurrent experiments

We have recently developed the use of the Time-Resolved Electric-Field-Induced Second Harmonic generation (TREFISH) technique to monitor photogenerated charge motion in complete OPV devices.[19,80] The technique has been used prior to study pristine conjugated polymer films[8,27,63] and is described in detail elsewhere.[8,19,81] Briefly, the motion of photogenerated charges partially screens the electric field F created by the applied bias, resulting in a temporal change $\Delta F(t)$. This change can be measured optically by detecting the temporal change in the second harmonic intensity $\Delta I_{2H}(t) \propto \Delta F^2(t)$, for example using a photomultiplier tube. $\Delta F(t)$ can be converted to extracted charge as outlined in our earlier work.[19] To extend the temporal range, TREFISH measurements are complemented by a simultaneous (i.e. using the same pump pulse) measurement of the transient photocurrent, allowing to probe a wide temporal range 100 fs – 10 μs (**Figure 5**). Using this technique, all of the relevant time scales for charge transport can be monitored in complete OPV devices with optical (i.e. sub-picosecond) temporal resolution.

We have previously confirmed the generality of this technique by experiments on polymer:fullerene,[19–21,44,45] polymer:polymer[20] and small molecule based[22] OPV devices (Figure 5). In addition, we have shown that OPV device photocurrent-voltage curves under steady-state AM1.5 illumination or under continuous monochromatic laser illumination (785 nm in this case) can be reconstructed using time-resolved measurements (Figure 5d). As such, the time-resolved photogenerated charge extraction kinetics in Figure 5 show charge extraction as it occurs in OPV devices operating under steady-state illumination conditions.

Experimental data such as in Figure 5, spanning all of the relevant time scales for charge transport, are ideally suited for testing the validity of charge transport models. Any model which attempts to fit the time-resolved charge extraction experiments, must also reproduce the experimental field-dependence (i.e. *U* spanning from 0V to -5V in Figure 5c) using a single parameter set, thus severely constraining the model. We were able to successfully fit all of the experimental data shown above using 3D kMC simulations based on the GDM framework. The full details of the 3D kMC model are described in detail in the supplementary information of ref. [21].

The advantage of the kinetic Monte Carlo algorithm is that it does not contain implicit assumptions regarding quasi-equilibrium. Instead, the photogenerated charge carrier populations are allowed to thermalize as set by the carrier hopping parameters and the energetic disorder. Therefore, by fitting the model to the combined TREFISH and transient photocurrent experiments, statements whether the photogenerated carriers have (or have not) reached quasi-equilibrium during their presence in the OPV device can be made.

Figure 5 highlights the generality of this approach as reasonably good fits to experimental data were obtained. Note that fitting such a wide temporal range is one of the hallmarks of the GDM framework. In contrast, the shaded areas in Figure 5a indicate the outcome if a simplified model was used instead for TQ1:$PC_{71}BM$ (1:2.5). The simplified model is based on experimentally measured quasi-equilibrium mobility values using a single technique (pCELIV) which probes

the mobility of almost fully thermalized charge carriers.[19] The main assumptions of the simplified model are: 1) all of the photogenerated charge carriers have an identical mobility. 2) The mobility of the photogenerated charges is time-independent as they are assumed to be in quasi-equilibrium. The simplified model captures neither the rapid extraction of the photogenerated charges nor the shape of the experimental extraction kinetics (Figure 5a).

In the following sections we show that due to the stochastic and non-equilibrium nature of carrier hopping in disordered media both assumptions of the simplified model are insufficient to explain the Figure 5a experiments. The photogenerated charge populations are instead characterized by a wide distribution of extraction times – charge transport is dispersive (contrary to the 1st assumption of the simplified model). In addition, the mobility of the photogenerated charges is in fact time-dependent, as predicted by GDM (Figure 1 and 2) and confirmed by TA (Figure 4), due to the gradual thermalization of the photogenerated charges in their respective DOS (contrary to the 2nd assumption of the simplified model). Both of these aspects are discussed in sections 5.2 and 5.3.

Figure 5a and 5c stress the need for sufficient temporal resolution when making statements about the (ir)relevance of (non)equilibrium carrier transport. Recently Le Corre et al. argued that charge extraction in OPV devices can be described by a drift-diffusion model using quasi-equilibrium mobility values estimated from charge extraction experiments with ~0.1 µs temporal resolution.[82] Figure 5a and 5c clearly show that at 0.1 µs a significant fraction of photogenerated charges may have already been extracted, precluding any meaningful statements about those charges. Measurements with insufficient temporal resolution probe only the slowest (most thermalized) subset of the photogenerated carrier population, which is not necessarily meaningful for OPV device operation. Explicit 3D kMC simulations of the experiments by Le Corre et al. confirmed this view[83] – only measurements spanning all relevant time scales are suited for making conclusive statements regarding charge transport in organic electronic materials.

5.2. Dispersion in photogenerated charge extraction times

Since carrier hopping between localized sites in an organic semiconductor is stochastic process, even charges traversing the same distance to the electrodes will be extracted at different times following photoexcitation. We have previously shown[19] that the distribution of extraction times can be obtained from TREFISH and transient photocurrent experimental data as follows: since the experimental trace in Figure 5a represents the integral of the charge extraction distributions, by taking a log derivative $dQ(t)/d(\log(t))$ of the experimental trace, the distribution of extraction times can be obtained. This is illustrated in **Figure 6**.

Since charges in an OPV device are photogenerated at different distances from the extracting electrodes, the broadening in Figure 5a extraction kinetics is at least in part due to a different transport distance. However, this broadens the extraction time distribution only by ~2 orders of magnitude in time, as can be inspected from the simplified quasi-equilibrium model in Figure 5a, where the first electrons are extracted at ~1 ns, whereas the last electron is extracted at ~100 ns. In contrast, the experimentally estimated distribution in Figure 6b spans 5-6 orders of magnitude in time and is due to the dispersive nature of charge transport in disordered media.

The wide distribution in extraction times reveals several key features regarding photocurrent in OPV devices. First of all, kinetic Monte Carlo simulations suggest that the charge extraction distributions obtained by pulsed laser excitation are identical to those obtained under continuous illumination (Figure 6a middle panel). As such, these results show that, in principle, the distribution of extraction times in OPV devices operating under continuous 1 sun illumination conditions can be determined by pulsed laser measurements using sufficiently low pump-fluence. This further corroborates the relevance of this time-resolved data to steady-state device operation, in addition to the good overlap with photocurrent-voltage curves in Figure 5d.

Most importantly, due to dispersion, mean extraction times are a particularly bad measure of the actual charge extraction in OPV devices. The vertical colored bars in the middle panel of

Figure 6a indicate the mean extraction time for the holes (red vertical bar) and for the electrons (blue vertical bar). At the mean extraction time about 80-90% of all the photogenerated holes/electrons have been extracted already. In addition, by inspecting the charge extraction histograms it is clear that 50% of the holes/electrons (the early time part of the histogram, to the left of the peak maximum) are extracted orders of magnitude faster than the remaining 50%. This idea, albeit using lower temporal resolution TOF measurements, was independently confirmed in ref. [13]. These experiments illustrate that even a well-defined (time-dependent) mean mobility, is of limited use in view of the large dispersion.

Most experimental techniques that estimate the charge carrier mobility are largely insensitive to dispersion and only provide an estimate for the mean mobility of the corresponding charge carrier population. However, it is very challenging to account for the associated spread around this mean. For practical reasons, we will further only discuss the log-mean carrier mobility (situated at the peak maximum of the charge extraction histogram). Nevertheless, the large dispersion in extraction times must be at least considered when analyzing charge transport in organic semiconductors.

5.3. Time-dependent photogenerated carrier mobility

In addition to dispersion in charge extraction times, the simplified quasi-equilibrium model also underestimates the rapid extraction of photogenerated charges (Figure 5a). In our initial publication,[19] we have used 3D kMC simulations to show that the photogenerated charges undergo gradual thermalization (Figure 6a). In fact, the relevant time scales were very similar to those in earlier published TA thermalization data (Figure 4). According to the GDM framework, such gradual thermalization leads to a time-dependent mean carrier mobility which decreases due to an increasing number of upward hops required for charge transport at longer time scales following photoexcitation. In this section, we describe complementary experimental evidence supporting the notion that photogenerated carriers indeed undergo gradual

thermalization in their respective DOS, and that charge extraction in OPV devices is a transient non-equilibrium process governed by a time-dependent carrier mobility.

To test this conclusion, charge motion on time scales from sub-picoseconds to tens of microseconds must be probed. This is particularly challenging, since most time-resolved techniques probe the dynamics of photo-excited species only over a limited temporal range, providing only a snapshot of the full dynamics. We have employed several techniques with an overlapping temporal range; an overview of the collected results is shown in **Figure 7**, experimentally confirming that photogenerated charge extraction in disordered organic semiconductors, as revealed by TREFISH and transient photocurrent measurements in Figure 5 and corroborated by TA data in Figure 4, is indeed governed by the gradual thermalization of photogenerated charges (Figure 7).

Figure 7a shows the time-resolved GSB redshift ΔE for TQ1:$PC_{71}BM$ (1:2.5) and PCDTBT:$PC_{61}BM$ (1:2), taken from the earlier discussed data in Figure 4a and 4b. Both the magnitude of thermalization losses and the pump-fluence independence observed in experiments can be successfully fitted using 3D kMC (Figure 7a red traces).[21] Figure 7b shows the corresponding time-dependent mobility simulations that originate from independently fitting the TREFISH and transient photocurrent data on the same TQ1:$PC_{71}BM$ (1:2.5) device in Figure 5a. Note that the time-dependent mobility is also pump-fluence independent, highlighting the coupling of photogenerated carrier thermalization (Figure 4) to hopping motion (Figure 5 and 7), as explained in section 2.3 describing the GDM framework: when out of equilibrium, concentration effects related to DOS state-filling are considerably less important.

Figure 7b shows good agreement between the simulated photogenerated carrier time-dependent mobility and several time-resolved and steady-state experiments: TRTS, TRMC combined with TA, pCELIV and SCLC. Note that the simulated time-dependent mobility is also based on experimental data, since it was obtained from the 3D kMC fits to the TREFISH and transient photocurrent experiments on an OPV device in Figure 5a. As such, Figure 7 highlights that

although the different transient techniques probe different time scales and even different signals (energy vs. charge motion), they are mutually consistent, as they monitor the same physical mechanism governing charge motion – charge carrier hopping and thermalization in the disorder broadened DOS. In later work (sections 6 and 7) we have extended these results to polymer:polymer[20] devices and small molecule based OPV devices with varying morphology.[22] As such, Figure 7 unifies commonly employed opto-electric techniques that probe charge motion in disordered organic semiconductors in a consistent framework.

Having established that the photogenerated carrier mobility in disordered OPV blends is time-dependent, we dedicate the next two sections to discuss several relevant mobility measurement techniques. We first focus on TRTS and TRMC, since these techniques can monitor the motion of photogenerated charges at time scales shorter than ~1 μs, while charges are undergoing thermalization (Figure 7).

5.4. Time-resolved terahertz spectroscopy (TRTS)

The use of THz radiation as a probe allows monitoring of charge carrier mobility dynamics at the earliest time scales following photogeneration.[7] For OPV materials the measurement range typically spans 1-1000 ps, with the long-time limit set by the signal-to-noise ratio. This temporal window is particularly important for the investigation of photoinduced charge separation at the D/A interface,[61] followed by charge transport away from the interface.

Since TRTS measurements provide an estimate for the time-resolved photoconductivity $\Delta\sigma(t)$, to estimate the charge carrier mobility $\mu(t)$, the time-resolved charge density $n(t)$ must be independently obtained using for example TA measurements on the same film at an identical pump-fluence.[26] This is because $\mu(t) \propto \Delta\sigma(t)/n(t)$.

The mean TRTS mobility $\mu(t) = [\mu_e(t) + \mu_h(t)]/2$ is generally considered to be dominated by the hole mobility $\mu_h(t)$ in the polymer donor phase, and thus corresponds to the hole mobility. This assignment is based on the considerably lower electron $\mu_e(t)$ mobility in neat $PC_{61}BM$ on a time

scale of several picoseconds, as previously determined using time-resolved EA spectroscopy (μ_e = 0.5 × 10^{-2} cm^2 V^{-1} s^{-1} in the zero-field limit)[6,30] and TRTS measurements on APFO3:$PC_{61}BM$ blends (μ_e = 0.3 × 10^{-2} cm^2 V^{-1} s^{-1})[16]. Measurements on APFO3:$PC_{61}BM$ blends show increasing TRTS mobility with increasing polymer chain length,[16] whereas TRTS measurements on P3HT:$PC_{61}BM$ blends show only a minor effect of side chain regioregularity on TRTS mobility (μ = 0.1-0.4 cm^2 V^{-1} s^{-1}).[17] The observed TRTS mobility dependence on polymer chain length and the weak dependence on side chain regioregularity suggest that TRTS probes the hole mobility on the polymer backbone.

Although similar TRTS data as for P3HT and APFO3 are not available for TQ1:$PC_{71}BM$ (1:2.5) (Figure 7b), its TRTS mobility is also expected to be dominated by the hole mobility in the TQ1 polymer phase. This assignment is tentatively in agreement with TA measurements, where the redshift of the GSB, corresponding to hole thermalization, begins at a pump-probe delay of ~100 ps (Figure 7a). The TRTS mobility in TQ1:$PC_{71}BM$ (1:2.5) also begins to decrease at ~100 ps following photoexcitation (Figure 7b). The TRTS mobility data in Figure 7b could be indicative of the onset of hole thermalization, whereas the subsequent mobility decay may be tentatively assigned to inter-site hole hopping. At this point, this assignment is merely a hypothesis and further studies are required to test this idea.

A complementary way to interpret the TRTS data is by considering the THz pulse as a time varying (AC) electric field to which the photogenerated carriers respond. This is important to consider since carrier mobility in organic semiconductors is known to be strongly frequency-dependent.[84] When probed by a high-frequency THz electric field, the charge carriers drift only a short distance during the period of the wave, opening the possibility of hopping between DOS sites of similar energy, leading to an apparently high mobility. In contrast, at low frequency (e.g. during transport at a constant electric field) the charge carriers are transported over larger distances and are more prone to encounter high energy barriers (difficult hops), significantly reducing the charge carrier mobility. As such, the measured TRTS mobility

describes charge motion over relatively short length scales of the order of ~1 nm (ref. [85]), where transport through DOS sites of similar energy leads to an increase in carrier mobility. When accounting for the high-frequency probing (e.g. at THz frequencies ~10^{12} Hz), our kMC simulations came significantly closer to the experimental values than the essentially DC simulations shown in Figure 7b.[21] The finding that the high probing frequency makes the TRTS mobility appear less time-dependent is supported by earlier theoretical work on pristine materials, also employing the GDM framework.[86] The apparently time-independent TRTS mobility at the earliest time scales (1-100 ps), observed in typical OPV systems, may thus at least in part be due to the high frequency of the THz probe and not due to the complete absence of carrier thermalization. Further studies, disentangling the effect of the AC field on the observed kinetics, would elucidate the underlying photophysics.

5.5. Time-resolved microwave conductance (TRMC)

Following the earliest time scales of charge separation and motion away from the D/A interface, as probed by the TRTS technique, subsequent charge transport and recombination can be monitored by TRMC which spans the ~20 ns – 1 μs range following photoexcitation. This temporal range is particularly suited for the investigation of charge separation and transport at later time scales and over larger distances, as compared to those probed by TRTS. Similar to TRTS, TRMC provides an estimate for the time-resolved photoconductivity $\Delta\sigma(t)$ and therefore to estimate $\mu(t)$, complementary TA measurements on the same film at an identical pump-fluence are generally necessary, since $\mu(t) \propto \Delta\sigma(t)/n(t)$.

Due to the considerably lower frequency of the electric field in a microwave probe (GHz), compared to that in a Terahertz probe (THz), AC effects, due to the time-varying electric field of the microwave, are expected to be significantly less important in TRMC transients. Earlier work from other groups[84,86] and our own work[21] corroborate this observation. Therefore, the

measured TRMC mobilities in OPV films can be more directly compared to those obtained by other DC (constant applied electric field) mobility techniques. However, it has to be kept in mind that since TRMC probes charge motion only during a fairly limited temporal range, the photogenerated charges will traverse only a limited distance during this time. In other words, the TRMC technique probes the carrier mobility over some "local" spatial scale, similar to TRTS measurements. In that sense, the TRMC mobility may exceed that recorded by DC mobility techniques.

TRMC allows for additional means of detecting whether the photogenerated charges have reached quasi-equilibrium at the 20 ns – 1 μs time scales. For example, in TQ1:$PC_{71}BM$ (1:2.5) most of the photogenerated carrier thermalization has already taken place at these time scales and the photogenerated charges are close to, but not in quasi-equilibrium (Figure 7b). The presence of a non-equilibrium situation can be confirmed by pump-fluence dependent TRMC mobility measurements. Quasi-equilibrium carrier mobility in disordered organic semiconductors is known to be strongly dependent on carrier density,[52,67] whereas this is not necessarily the case when out-of-equilibrium, as explained in previous sections. Using TRMC measurements, we have shown that at 20 ns – 1 μs time scales the photogenerated carrier mobility in TQ1:$PC_{71}BM$ (1:2.5) is concentration-independent up to carrier densities of approximately ~1×10^{18} cm^{-3} (ref. [21]). This serves as complementary experimental proof that at time scales probed by TRMC the photogenerated carriers in TQ1:$PC_{71}BM$ (1:2.5) have not yet reached quasi-equilibrium.

In contrast, Savenije et al. have suggested that for regioregular-P3HT:$PC_{61}BM$ (rrP3HT:$PC_{61}BM$) blends the TRMC mobility is time-independent at these time scales.[28] In general, the lower the energetic disorder of the material, the less important are non-equilibrium effects due to carrier thermalization.[20] It may be expected that the TRMC mobility in rrP3HT:$PC_{61}BM$ is time-independent at least in part due to the lower energetic disorder of rrP3HT:$PC_{61}BM$, compared to that in TQ1:$PC_{71}BM$. Such measurements, particularly on novel

material systems, would be particularly interesting to check for the importance of non-equilibrium phenomena. Note that RC limited charge extraction experiments are not particularly well suited for this purpose as discussed in section 5.1.

6. Relation to mobility measurements without photoexcitation

Previously discussed experimental results have thus far focused on the time-dependent mobility of photogenerated charges following an excitation by a laser pulse. Alternatively, mobility measurements can also be performed under steady-state conditions in the dark (i.e. without photoexcitation). In this case the charge carriers are injected from the electrodes and, after traversing the OPV film, extracted at the second electrode. The relevance of the most widely adopted mobility measurement technique used to describe operating OPVs, space-charge limited currents (SCLC), relies on the assumption that the mobility of photogenerated charges is the same, or least comparable to that of charges injected from the electrodes in the dark. Here, we summarize the main findings from our earlier work,[20] which suggests that for sufficiently disordered organic semiconductors (i.e. in most cases), this notion is questionable at best.

6.1. Space-charge limited currents (SCLC)

Space-charge-limited currents (SCLC) is a commonly used technique to determine the steady-state charge carrier mobility in organic semiconductors. The SCLC method relies on the use of electrodes that are Ohmic for only one type of carrier (hole- or electron-only SCLC), facilitating the injection of the selected carrier from the electrode into the OPV film. The injected charge carriers, following charge transport through the film, are extracted at the second electrode. Device geometry is similar to that of an OPV device and, using suitably chosen electrodes, the hole or the electron mobility can be determined. This is advantageous, as it is generally quite challenging to distinguish the electron and hole contributions in time-resolved experiments.

In its simplest form, the theory of SCLC predicts a current that is proportional to the applied voltage squared $j \propto U^2$, allowing the mobility to be extracted from a linear fit on a double-log scale. Despite it being well-known that this procedure is prone to large errors due to the density- and field-dependence of the charge carrier mobility in organic semiconductors, this method is still widely used.[87] We have recently made our software, accounting for the density- and field-dependent carrier mobility, openly available.[50] It allows GUI-based extraction of mobilities (and hopping parameters) from (temperature-dependent) SCLC data using a variety of models, including the GDM framework, and enabling fully automated least-squares fitting of SCLC data with minimal error, user input and SCLC data analysis time.

Generally speaking, the SCLC method probes the mobility of charges situated at their quasi-equilibrium energy in the DOS. In contrast, the photogenerated charges are temporarily situated at higher DOS energies and undergo thermalization which boosts their motion, as schematically shown in **Figure 8**. The fact that ultrafast time-resolved measurements often provide higher mobility values than those measured by SCLC (Figure 1a) supports this schematic.

To experimentally test the above, we have explicitly compared the mobility of photogenerated charges, as determined by 3D kMC fitting to TREFISH and transient photocurrent measurements to data in Figure 5a and 5b, with the mobility of charges injected from the electrodes in the dark, as determined by SCLC.[20] These measurements were performed on TQ1:$PC_{71}BM$ (1:2.5) and its non-fullerene analog TQ1:N2200 (2:1) (Figure 8). Successful 3D kMC fits to the time-resolved measurements in Figure 5a and 5b allowed the extraction of the time-dependent photogenerated hole and electron mobilities in both blends (lines in Figure 8a). Similarly, by fitting the SCLC data (Figure 8c) using a model based on the GDM framework, accounting for carrier-density- and field-dependent mobility, enabled estimating the injected carrier mobility at comparable carrier densities (shaded areas in Figure 8a). The photogenerated carrier mobility exceeds the SCLC mobility by several orders of magnitude, especially at early times following photoexcitation (Figure 8a). Given the significant difference, it is questionable

whether photogenerated charge transport can be characterized by the SCLC method, particularly for materials with a large disorder.

Generally speaking, the error in using a quasi-equilibrium carrier mobility is expected to be lower for materials with lower energetic disorder. Since the GDM formalism used here applies to a wide range of disordered organic semiconductors, 3D kMC simulations allow to predict the error for materials with different disorder values than those measured for TQ1:$PC_{71}BM$ (1:2.5) and TQ1:N2200 (2:1). The inset of Figure 8d illustrates that with decreasing energetic disorder, the mobility of photogenerated charges becomes less time-dependent, and thus the error in using the SCLC mobility rather than the time-dependent traces, becomes less pronounced.

For materials with significant disorder, photogenerated carriers will, in a given time t after photogeneration, traverse larger drift distances than quasi-equilibrated carriers, resulting in a significant error in drift distance $\Delta d(t)$, which quantifies the drift distance by which a quasi-equilibrated carrier is lagging behind a photogenerated carrier (see Figure 8b schematic). Figure 8d shows the predicted error for a range of hypothetical materials with the indicated disorder at short-circuit (1V / 100nm) and at maximum-power point (0.2V / 100nm) conditions at a photogenerated carrier drift distance of $d_{\text{photo}}(t) = \frac{U_{\text{eff}}}{L}\int_0^t \mu_{photo}(t)dt$ = 50 nm (i.e. corresponding to a 100 nm device), where U_{eff} is the applied voltage corrected by device built-in voltage, L is the active layer thickness and $\mu_{\text{photo}}(t)$ is the time-dependent photogenerated carrier mobility. The error is larger at short-circuit conditions, as the gain in drift distance with increasing electric field strength U/d is larger for the photogenerated charges. The error is decreases with decreasing disorder, since the DOS distribution narrows, making $\mu(t)$ less time-dependent (Figure 8d inset). For low disorder values thermalization effects on carrier transport become less important and tends to zero in the limit of low disorder ~50 meV. As we will show in section 7.1, on basis of our experimental findings, only neat C_{60} has such low disorder.

Although it is not entirely evident what error in $d_{photo}(t)$ is acceptable in practice, in ref. [20] we have, for illustrative purposes, chosen 15% of the average carrier drift distance in a typical 100 nm thick photoactive layer (i.e. 15% × 100 nm / 2 = 7.5 nm), as marked in Figure 8d by the green shaded area. This shows that at MPP conditions (0.2V / 100nm) the use of SCLC mobility data, or other mobility data obtained by slow time-resolved or quasi-equilibrium measurement techniques (e.g. transient photocurrent, pCELIV or TOF), is acceptable only for materials with a sufficiently low energetic disorder (σ < 71 meV). The blends studied by us, TQ1:$PC_{71}BM$ (1:2.5), TQ1:N2200 (2:1), MDMO-PPV:$PC_{61}BM$ (1:4), and PCDTBT:$PC_{61}BM$ (1:2), were all found to be outside this range.[20,21,44] Furthermore, at short-circuit conditions, corresponding to higher electric fields strengths than at MPP, even lower disorder values (σ < 56 meV) are required for a reliable description. As the majority of previously studied OPV blends typically have an energetic disorder larger than σ = 56-71 meV or similar, these simulations emphasize that using SCLC mobility data for describing disordered OPVs is prone to large errors even at relatively weak electric fields. Quasi-equilibrium mobility data are expected to be reliable only for materials with a sufficient low energetic disorder and highly inaccurate for materials with moderate to high energetic disorder. Whether this holds true for modern OPV materials, particularly those based on novel non-fullerene acceptors, remains to be experimentally tested.

7. Charge transport in pure and mixed phases

Organic BHJ solar cells are known to have complicated multi-length scale morphologies.[88–91] The experimental data discussed so far focused on rather amorphous D/A blends which were analyzed assuming that the photoactive film can be treated as an effective medium – the nanoscale morphology of the BHJ film was not explicitly accounted for. In our initial publications,[19–21] this was done to limit the number of experimentally unknown 3D kMC parameters.

In order to understand how the morphology of the BHJ affects non-equilibrium charge motion, it would be desirable to investigate a set of samples where a rather well-defined BHJ morphology is varied in a controlled manner. This was, at least to some extent, accomplished in ref. [22], where carefully co-sublimed BHJs, based on small-molecule donor/acceptor mixtures, were investigated. Although similar data, investigating the effect of donor/acceptor mixing on charge transport is available in literature[18,88,89,92–94], previously reported studies are mainly semi-quantitative in the sense that they do not answer the question of how pure the neat domains have to be to facilitate efficient charge transport. The well-defined sample morphology and the unique temporal resolution and range offered by the combination TREFISH and transient photocurrent measurements in ref. [22] enabled quantitative analysis. In addition, in ref. [22] we have used direct CT photoexcitation, to confirm that even under CT excitation the photogenerated charges still undergo thermalization, c.f. Figure 1b. Three important insights have been revealed that will be discussed in the sections that follow.

7.1. Effects of phase purity on charge transport

To elucidate the impact of varying levels of domain continuity, purity and D/A mixing on charge transport we have studied co-sublimed OPV blends where the molar fraction of α-sexithiophene (α-6T) in a buckminsterfullerene (C_{60}) matrix was varied from homogeneously diluted α-6T (<10 mol%), to a regime where α-6T starts forming isolated aggregates (>10-25 mol%) or is strongly aggregated (50 mol%). In other words, we have varied the distance between isolated α-6T sites and the level of disruption of the C_{60} phase in a controlled manner. The α-6T:C_{60} system can be considered as a model system for studying the mixed donor-acceptor phase in general OPV. By a combination of TREFISH and transient photocurrent experiments, complemented with simulations based on the GDM framework, we have quantified how D/A mixing affects the charge extraction kinetics, see **Figure 9**.

To the best of our knowledge, these measurements are the first experimental demonstration of following the transient motion of charges photogenerated in the CT manifold in a complete OPV device, corroborating previously reported internal quantum efficiency (IQE) measurements[95] showing efficient extraction of such charges. Model fittings to Figure 9a data reveal that also charges photogenerated in the CT manifold undergo thermalization (Figure 9c), which is due to a large number of low energy DOS sites below the CT energy, c.f. Fig 1b.[22]

The transient extraction measurements reveal two extraction plateaus (Figure 9), most clearly visible for the device with 10 mol% donor. Charge carrier mobilities of μ = 0.5 cm^2 V^{-1} s^{-1} and $\mu = 6 \times 10^{-5}$ cm^2 V^{-1} s^{-1}, respectively, are expected on basis of the approximate temporal position of the observed plateaus (black dashed lines in Figure 9a) in the time-resolved charge extraction data. We have attributed the latter part of the transients to hole transport via isolated α-6T sites (the transport mechanism is described in section 7.2), as confirmed by complementary hole-only mobility measurements using SCLC (Figure 9c inset), giving $\mu_h = 6 \times 10^{-5}$ cm^2 V^{-1} s^{-1} at 10 mol% donor. On basis of the high electron mobility reported in neat C_{60} crystals (μ_e = 0.5 cm^2 V^{-1} s^{-1})[96], the early part of the transients can be attributed mainly to the extraction of electrons. However, as we have shown in ref. [22], a small fraction of holes (0-20%, depending on the electric field in the OPV device, i.e. applied bias) is also very rapidly extracted via C_{60} (discussed in section 7.2).

The assignment of electron/hole extraction to the first/second plateaus in the transient extraction kinetics is similar to that used for polymer/fullerene[19] and polymer/polymer[20] blends. This highlights that hole extraction in OPV devices, based on either polymer/fullerene, polymer/polymer or small molecule blends, is generally significantly slower than electron extraction. It would be insightful to investigate whether this is also the case for modern systems, particularly those employing state-of-the-art non-fullerene acceptors.

The increasingly convex shape of the electron extraction transients with increasing α-6T content indicates that α-6T addition disrupts the C_{60} phase, increasing its energetic disorder

(Figure 9b). An independent study using Grazing Incidence X-Ray Diffraction (GIXD) measurements corroborated this result: at 25-50 mol% donor the diffraction rings corresponding to polycrystalline C_{60} become absent, indicating amorphous C_{60}.[97] Figure 9c shows the corresponding effect on the photogenerated electron mobility (blue traces). With increasing α-6T content electron transport undergoes a transition from non-dispersive (time-independent μ_e) to dispersive charge transport (time-dependent μ_e). This shows that, depending on the sample morphology, both charge transport regimes (non-equilibrium versus quasi-equilibrium) are possible in the same material. Note also the consistency between the disorder values for C_{60} in Figure 9b for which Figs. 9a-c show (non-)dispersive transport (10 mol% α-6T in C_{60}), and the (approximate) thresholds for dispersive behavior discussed in sections 5 and 6.

More concretely, donor addition below 10 mol% does not significantly hinder electron transport in the C_{60} phase – a quasi-equilibrium (long-time) electron mobility of the order of μ_e = 1-2 cm^2 V^{-1} s^{-1} is retained (Figure 9c), similar to the reported electron mobility in neat C_{60} crystals.[96] On the other hand, at higher than 10 mol% donor fractions, the quasi-equilibrium electron mobility is roughly an order of magnitude lower (μ_e = 0.08 cm^2 V^{-1} s^{-1} at 25 mol% donor) than at low donor content. Therefore, the C_{60} phase may be considered as effectively "pure" for electron transport at donor content below 10 mol%. Surprisingly, increasing the donor content has a rather weak effect on hole extraction, with very similar hole mobilities in the range of 5.7-50 mol% donor (Figure 9c). Hole extraction is poor only at very low donor content of 1.5 mol%. The responsible physical mechanism, governing hole transport in these low donor content OPV blends, is discussed in the next section.

7.2. Charge transport by long-range tunneling in low donor content OPV blends

We have also investigated charge transport α-6T:C_{60} blends with low donor content (1.5% and 5.7% molar dilution). These systems are rather peculiar, as despite the low donor content and lack of an interconnected donor network, they produce rather efficient OPV devices.[98,99] To

study OPV systems with low donor content, we have selected the transient measurement conditions to be such that the hole was initially situated on an isolated α-6T site (**Figure 10**) – the laser pump wavelength was selected to only excite the CT manifold. As such, the starting situation of the measurement was expected to be an immobile hole on an isolated donor molecule. The electron is rapidly extracted via C_{60}.

Given the experimental conditions and considering the strongly localized nature of charges in organic semiconductors, hole motion between isolated donor sites that are several nanometers apart (~3.4 nm on average at homogeneous 5.7% molar dilution[22]) should be quite unlikely. On the contrary, using transient measurements, we have experimentally shown that efficient long-range hole tunneling through several C_{60} molecules occurs over roughly ~4 nm distance.[22] This is clearly visible when comparing the transient extraction kinetics at 1.5% and 5.7% molar dilution (corresponding to mean center-to-center distances between isolated α-6T decreasing from roughly ~5.3 nm to ~3.4 nm, respectively), revealing a strong increase in the hole extraction peak at long time delays when the average distance between α-6T is decreased (Figure 10a). By systematically investigating 18 different donor materials diluted to ~6 mol% in a C_{60} matrix, Spoltore et al. have recently confirmed the generality of our proposed charge transport mechanism – long-range hole tunneling between non-nearest-neighbor donor molecules;[100] whereas using ab initio modeling Symalla et al. have recently suggested that charge transport in such guest-host systems is mediated by the coherent process of molecular superexchange.[101]

The combined transient and SCLC dataset in Figure 9c shows that hole transport between isolated donor sites takes place with a reasonably high hole mobility (μ_h = 5-15 × 10^{-5} cm^2 V^{-1} s^{-1} for 5.7-50 mol% donor). Since at low donor content (<10 mol%) electron transport in the C_{60} phase is unperturbed (μ_e = 2 cm^2 V^{-1} s^{-1}), this data shows that C_{60} domains containing only a trace amount of material with a donating character enable ambipolar transport. This has

several implications. First, the general notion that a continuous donor network is strictly necessary for hole transport in OPV devices is not entirely correct. Secondly, the commonly used terms of "pristine", "neat" or "pure" phase are rather ambiguous. For example, C_{60} domains with 10 mol% donor can be viewed as effectively pure for electron transport, whereas, from the hole perspective, the same material, containing 90 mol% of C_{60}, would be typically termed as "not pure at all". However, the data shows that even at such low amounts of isolated donor, the hole mobility is similarly high as at 50 mol% donor (μ_h = 6-11×10^{-5} cm^2 V^{-1} s^{-1} for 10-50 mol% donor). Therefore, these results question the relevance of "pristine" phases (and the correct use of the term in the field) and whether a continuous interpenetrating D/A network is absolutely necessary for charge transport.

In addition, the transient data revealed that while the majority of the photogenerated holes in α-6T:C_{60} is transported between isolated donor sites by long-range hole tunneling through C_{60}, at high reverse bias a small fraction (0-20%) of the photogenerated holes can be transferred to and extracted via the C_{60} phase.[22] The possible importance of ambipolar transport in the fullerene phase of OPV devices has been previously highlighted by several groups,[94,102,103] challenging the general view that hole transport is strictly facilitated by the donor, and electron transport by the fullerene acceptor. The fraction of holes extracted via C_{60} can be quantified from the ratio in the extraction plateaus in the transient kinetics (Figure 10c). Since the photogenerated carriers are generated in pairs, a ratio of 0.5 means that the early time plateau is entirely dominated by the extraction of electrons. Figure 10c reveals that when the reverse bias is increased the fraction of charges extracted at early times increases above 50% (thick black horizontal line in Figure 10c). In view of the previously reported high hole mobility in neat C_{60} crystals (μ_h = 2 cm^2 V^{-1} s^{-1})[22], the bias-dependent increase of the early time extraction plateau was attributed to the rapid extraction of holes via C_{60}.

We have suggested that hole de-trapping at high reverse bias occurs by Fowler-Nordheim-type tunneling[104] through a triangular energy barrier (Figure 10d). Additional bias-dependent

measurements and 3D kMC simulations, accounting for the sample morphology, have revealed that this process is only relevant at high reverse bias and not important for operating OPV devices.[22] At field strengths relevant to OPV devices (e.g. short-circuit conditions), facile hole capture by isolated donor sites will rapidly reduce the hole fraction transported in C_{60} to zero. Upon trapping on isolated α-6T, low electric fields are insufficient to overcome the large energy barrier for hole de-trapping by direct tunneling to C_{60}, forcing all holes to move by long-range tunneling between isolated donor sites (Figure 1b) or thermal de-trapping. In view of this, and at least in case of small molecule-donor and neat fullerene (C_{60} or C_{70}) OPV devices, hole extraction only via the fullerene phase can be ignored. However, long-range hole tunneling via isolated sites of a material with a donating character, for example donor molecules or impurities, must be considered. It remains to be seen to which degree these results can be transferred to other systems, for example non-fullerene acceptors, and although some initial studies exploring the limits of this charge transport mechanism have been carried out,[22,100,101,105] the limits of long-range tunneling between non-nearest-neighboring molecules are yet to be explored.

8. Outlook

In this progress report, we have shown that photogenerated charge motion in a variety of organic bulk heterojunction solar cells, including polymer:fullerene, polymer:polymer and small molecule blends, is governed by non-equilibrium phenomena. Slow thermalization in the disorder-broadened DOS is shown to result in a time-dependent photogenerated carrier mobility and strong dispersion in charge extraction times. Since thermalization typically does not complete before charge extraction, quasi-equilibrium mobilities, and models based on those, such as most implementations of the drift-diffusion model, are expected to be of limited relevance to describe the photogenerated charge extraction kinetics. Incomplete thermalization in thin films (typically ~100 nm for OPV devices) naturally brings up the question whether (and how) non-equilibrium phenomena affect device V_{OC}. Since voltage losses are to a large extent

responsible for the lower power conversion efficiencies of OPV versus inorganic PV,[33] this question is of utmost importance.

The current state-of-the-art interpretation of V_{OC} in OPV devices is based on reciprocity relations,[106] relating CT light-emission and absorption,[95,107,108] which assume detailed balance and thermal equilibrium under operational conditions. These schemes have been extremely successful in describing a range of experimental findings on a large number of OPV systems,[95,107,108] suggesting correctness of the underlying assumptions. On the other hand, the assumption of thermal equilibrium appears to be at odds with the fact that the majority of the photogenerated charges do not thermalize before extraction, even when energetic disorder is relatively small. To solve this apparent contradiction, there is a need for a framework that allows to calculate device V_{OC}, while simultaneously accounting for all implications of slow and possibly incomplete photogenerated carrier thermalization as observed by time-resolved experiments. The computational load of 3D kMC models that account for the presence of Ohmic contacts has, at least in our case, so far prohibited running such V_{OC} simulations.

The question to which extent non-equilibrium phenomena must be accounted for, can also be raised for the recombination of photogenerated charges in OPV. Above, it has been shown that charge separation (i.e. avoiding geminate and non-geminate recombination) is facilitated by the fast kinetics associated with thermalization, enabling (re)dissociation of CT pairs before recombination (Figure 4d). It may therefore be expected that recombination rates at short times following photogeneration are time-dependent. Indeed, a dispersive bimolecular recombination rate has been observed for the amorphous PCDTBT:$PC_{71}BM$ system by Kurpiers et al.[109] and earlier for TQ1:$PC_{71}BM$.[64] In contrast, in recent work focusing on TQ1:$PC_{71}BM$ device operation, it is demonstrated that under steady-state conditions, bimolecular recombination is instead governed by the equilibrium rate.[110] While this does not mean that all photogenerated charges in the operational solar cell are thermalized, it does indicate that recombination under steady-state predominantly proceeds through the thermalized fraction of charges remaining in

the device, whereas the non-thermalized fraction is extracted. This illustrates that while energetic disorder is generally detrimental for OPV devices, its effects are mitigated by transient effects and dispersion: extraction proceeds faster and with less recombination than would be expected for completely thermalized carrier populations. Likewise, incomplete thermalization of photogenerated charges may be expected to reduce the otherwise negative effect of disorder on V_{OC}.[111] Integrating these notions into a fully quantitative, and preferably predictive device model that can fit both transient fs-µs dynamics and current-voltage (IV) curves is a challenge of significant relevance.

Full material names

α-6T (Alpha-sexithiophene).
APFO3 (Poly[2,7-(9-di-octyl-fluorene)-alt-5,5-(4',7'-di-2-thienyl-2',1',3' benzothiadiazole)]).
C_{60} (Buckminsterfullerene).
ITO (Indium tin oxide).
MDMO-PPV (Poly[2-methoxy-5-(30,70-dimethyloctyloxy)-1,4-phenylene vinylene]).
N2200 (Poly[N,N'-bis(2-octyldodecyl)naphthalene-1,4,5,8-bis(dicarboximide)-2,6-diyl-alt-2,2'-bithiophene-5,5'-diyl]).
OC1C10-PPV (Poly[2-methoxy-5-(3',7'-dimethyloctyloxy)-p-phenylene vinylene]).
$PC_{61}BM$ ([6,6]-phenyl-C_{61}-butyric acid methyl ester).
$PC_{71}BM$ ([6,6]-phenyl-C_{71}-butyric acid methyl ester).
PCDTBT (Poly[N-11''-henicosanyl-2,7-carbazole-alt-5,5-(4',7'-di-2-thienyl-2',1',3' benzothiadiazole)]).
PEDOT:PSS (Poly[3,4-ethylene- dioxythiophene]:polystyrene sulfonate).
PVK (Poly-n-vinylcarbazole).
rrP3HT (Regioregular Poly[3-hexylthiophene-2,5-diyl]).
TNF (Trinitrofluorenone).
TQ1 (Poly[2,3-bis-(3-octyloxyphenyl)quinoxaline-5,8-diyl-alt-thiophene-2,5-diyl]).

Acknowledgements

A.M. gratefully acknowledges support from the Knut and Alice Wallenberg Foundation (KAW 2016.0494) for Postdoctoral Research at Stanford University. We thank Zhengrong Shang and Yoeri van de Burgt for feedback on the manuscript draft.

Received: ((will be filled in by the editorial staff))
Revised: ((will be filled in by the editorial staff))
Published online: ((will be filled in by the editorial staff))

References

[1] Y. Liu, J. Zhao, Z. Li, C. Mu, W. Ma, H. Hu, K. Jiang, H. Lin, H. Ade, H. Yan, *Nat. Commun.* **2014**, *5*, 5293.

[2] W. Zhao, D. Qian, S. Zhang, S. Li, O. Inganäs, F. Gao, J. Hou, *Adv. Mater.* **2016**, *28*, 4734.

[3] X. Che, Y. Li, Y. Qu, S. R. Forrest, *Nat. Energy* **2018**, *3*, 422.

[4] O. Inganäs, *Adv. Mater.* **2018**, *1800388*, 1.

[5] Z. Tang, Z. Ma, A. Sánchez-Díaz, S. Ullbrich, Y. Liu, B. Siegmund, A. Mischok, K. Leo, M. Campoy-Quiles, W. Li, K. Vandewal, *Adv. Mater.* **2017**, *29*, 1702184.

[6] J. Cabanillas-Gonzalez, T. Virgili, A. Gambetta, G. Lanzani, T. D. Anthopoulos, D. M. De Leeuw, *Phys. Rev. Lett.* **2006**, *96*, 106601.

[7] H. Němec, P. Ňuel, V. Sundström, *J. Photochem. Photobiol. A Chem.* **2010**, *215*, 123.

[8] A. Devižis, A. Serbenta, K. Meerholz, D. Hertel, V. Gulbinas, *Phys. Rev. Lett.* **2009**, *103*, 027404.

[9] T. J. Savenije, A. J. Ferguson, N. Kopidakis, G. Rumbles, *J. Phys. Chem. C* **2013**, *117*, 24085.

[10] N. Christ, S. W. Kettlitz, S. Züfle, S. Valouch, U. Lemmer, *Phys. Rev. B - Condens. Matter Mater. Phys.* **2011**, *83*, 195211.

[11] A. J. Mozer, G. Dennler, N. S. Sariciftci, M. Westerling, A. Pivrikas, R. Asterbacka, G. Juka, *Phys. Rev. B - Condens. Matter Mater. Phys.* **2005**, *72*, DOI 10.1103/PhysRevB.72.035217.

[12] A. Baumann, J. Lorrmann, D. Rauh, C. Deibel, V. Dyakonov, *Adv. Mater.* **2012**, *24*, 4381.

[13] J. Lorrmann, M. Ruf, D. Vocke, V. Dyakonov, C. Deibel, *J. Appl. Phys.* **2014**, *115*, 183702.

[14] M. A. Lampert, *Phys. Rev.* **1956**, *103*, 1648.

[15] P. N. Murgatroyd, *J. Phys. D. Appl. Phys.* **1970**, *3*, 308.

[16] C. S. Ponseca, H. Němec, N. Vukmirović, S. Fusco, E. Wang, M. R. Andersson, P. Chabera, A. Yartsev, V. Sundström, *J. Phys. Chem. Lett.* **2012**, *3*, 2442.

[17] M.-J. Sher, J. A. Bartelt, T. M. Burke, A. Salleo, M. D. McGehee, A. M. Lindenberg, *Adv. Electron. Mater.* **2016**, *2*, 1500351.

[18] V. Pranculis, Y. Infahsaeng, Z. Tang, A. Devižis, D. A. Vithanage, C. S. Ponseca, O. Inganäs, A. P. Yartsev, V. Gulbinas, V. Sundström, *J. Am. Chem. Soc.* **2014**, *136*, 11331.

[19] A. Melianas, V. Pranculis, A. Devižis, V. Gulbinas, O. Inganäs, M. Kemerink, *Adv. Funct. Mater.* **2014**, *24*, 4507.

[20] A. Melianas, V. Pranculis, Y. Xia, N. Felekidis, O. Inganäs, V. Gulbinas, M. Kemerink, *Adv. Energy Mater.* **2017**, *7*, 1602143.

[21] A. Melianas, F. Etzold, T. J. Savenije, F. Laquai, O. Inganäs, M. Kemerink, *Nat. Commun.* **2015**, *6*, 8778.

[22] A. Melianas, V. Pranculis, D. Spoltore, J. Benduhn, O. Inganäs, V. Gulbinas, K. Vandewal, M. Kemerink, *Adv. Energy Mater.* **2017**, *7*, 1700888.

[23] A. Melianas, Non-Equilibrium Charge Motion in Organic Solar Cells., Linköping University, **2017**.

[24] H. Bässler, *Phys. status solidi* **1993**, *175*, 15.

[25] R. Österbacka, A. Pivrikas, G. Juška, K. Genevičius, K. Arlauskas, H. Stubb, *Curr. Appl. Phys.* **2004**, *4*, 534.

[26] C. S. Ponseca, A. Yartsev, E. Wang, M. R. Andersson, D. Vithanage, V. Sundström, *J. Am. Chem. Soc.* **2012**, *134*, 11836.

[27] A. Devižis, K. Meerholz, D. Hertel, V. Gulbinas, *Chem. Phys. Lett.* **2010**, *498*, 302.

[28] T. J. Savenije, D. H. K. Murthy, M. Gunz, J. Gorenflot, L. D. A. Siebbeles, V. Dyakonov, C. Deibel, *J. Phys. Chem. Lett.* **2011**, *2*, 1368.

[29] D. H. K. Murthy, A. Melianas, Z. Tang, G. Juška, K. Arlauskas, F. Zhang, L. D. A. Siebbeles, O. Inganäs, T. J. Savenije, *Adv. Funct. Mater.* **2013**, *23*, 4262.

[30] A. Devižis, D. Hertel, K. Meerholz, V. Gulbinas, J. E. Moser, *Org. Electron. physics, Mater. Appl.* **2014**, *15*, 3729.

[31] P. Wurfel, *Physics of Solar Cells : From Basic Principles to Advanced Concepts*, Wiley-VCH, **2009**.

[32] F. E. Osterloh, *J. Phys. Chem. Lett.* **2014**, *5*, 3354.

[33] J. Yao, T. Kirchartz, M. S. Vezie, M. A. Faist, W. Gong, Z. He, H. Wu, J. Troughton, T. Watson, D. Bryant, J. Nelson, *Phys. Rev. Appl.* **2015**, *4*, 014020.

[34] S. D. Baranovskii, *Phys. Status Solidi Basic Res.* **2014**, *251*, 487.

[35] H. B. Anna Kohler, *Electronic Processes in Organic Semiconductors: An Introduction*, Wiley-VCH, **2015**.

[36] N. S. Sariciftci, L. Smilowitz, A. J. Heeger, F. Wudl, *Science (80-.).* **1992**, *258*, 1474.

[37] S. Gélinas, A. Rao, A. Kumar, S. L. Smith, A. W. Chin, J. Clark, T. S. Van Der Poll, G. C. Bazan, R. H. Friend, *Science (80-.).* **2014**, *343*, 512.

[38] F. E. Doany, D. Grischkowsky, *Appl. Phys. Lett.* **1988**, *52*, 36.

[39] J. R. Goldman, J. A. Prybyla, *Semicond. Sci. Technol.* **1994**, *9*, 694.

[40] H. Scher, E. W. Montroll, *Phys. Rev. B* **1975**, *12*, 2455.

[41] J. Orenstein, M. A. Kastner, *Solid State Commun.* **1981**, *40*, 85.

[42] T. Tiedje, A. Rose, *Solid State Commun.* **1981**, *37*, 49.

[43] S. D. Baranovskii, *Phys. Status Solidi Basic Res.* **2014**, *251*, 487.

[44] H. Van Eersel, R. A. J. Janssen, M. Kemerink, *Adv. Funct. Mater.* **2012**, *22*, 2700.

[45] I. A. Howard, F. Etzold, F. Laquai, M. Kemerink, *Adv. Energy Mater.* **2014**, *4*, 1301743.

[46] P. W. Anderson, *Phys. Rev.* **1958**, *109*, 1492.

[47] A. Miller, E. Abrahams, *Phys. Rev.* **1960**, *120*, 745.

[48] W. D. Gill, *J. Appl. Phys.* **1972**, *43*, 5033.

[49] C. Tanase, E. J. Meijer, P. W. M. Blom, D. M. de Leeuw, *Phys. Rev. Lett.* **2003**, *91*, DOI 10.1103/PhysRevLett.91.216601.

[50] N. Felekidis, A. Melianas, M. Kemerink, *Org. Electron.* **2018**, *61*, 318.

[51] R. A. Marcus, *Rev. Mod. Phys.* **1993**, *65*, 599.

[52] R. Coehoorn, W. F. Pasveer, P. A. Bobbert, M. A. J. Michels, *Phys. Rev. B - Condens. Matter Mater. Phys.* **2005**, *72*, 155206.

[53] E. Wang, J. Bergqvist, K. Vandewal, Z. Ma, L. Hou, A. Lundin, S. Himmelberger, A. Salleo, C. Müller, O. Inganäs, F. Zhang, M. R. Andersson, *Adv. Energy Mater.* **2013**, *3*, 806.

[54] Z. M. Beiley, E. T. Hoke, R. Noriega, J. Dacuña, G. F. Burkhard, J. A. Bartelt, A. Salleo, M. F. Toney, M. D. McGehee, *Adv. Energy Mater.* **2011**, *1*, 954.

[55] A. Hofacker, J. O. Oelerich, A. V. Nenashev, F. Gebhard, S. D. Baranovskii, *J. Appl. Phys.* **2014**, *115*, 223713.

[56] A. Hofacker, D. Neher, *Phys. Rev. B* **2017**, *96*, 245204.

[57] N. Felekidis, A. Melianas, M. Kemerink, *Phys. Rev. B* **2016**, *94*, 035205.

[58] V. Abramavicius, V. Pranculis, A. Melianas, O. Inganäs, V. Gulbinas, D. Abramavicius, *Sci. Rep.* **2016**, *6*, 32914.

[59] R. Noriega, A. Salleo, A. J. Spakowitz, *Proc. Natl. Acad. Sci.* **2013**, *110*, 16315.

[60] H. Němec, H. K. Nienhuys, E. Perzon, F. Zhang, O. Inganäs, P. Kužel, V. Sundström, *Phys. Rev. B - Condens. Matter Mater. Phys.* **2009**, *79*, 245326.

[61] P. A. Lane, P. D. Cunningham, J. S. Melinger, O. Esenturk, E. J. Heilweil, *Nat. Commun.* **2015**, *6*, 7558.

[62] D. A. Vithanage, A. Devižis, V. Abramavičius, Y. Infahsaeng, D. Abramavičius, R. C. I. MacKenzie, P. E. Keivanidis, A. Yartsev, D. Hertel, J. Nelson, V. Sundström, V. Gulbinas, *Nat. Commun.* **2013**, *4*, 2334.

[63] A. Devizis, K. Meerholz, D. Hertel, V. Gulbinas, *Phys. Rev. B - Condens. Matter Mater. Phys.* **2010**, *82*, 155204.

[64] L. M. Andersson, A. Melianas, Y. Infahasaeng, Z. Tang, A. Yartsev, O. Inganäs, V. Sundström, *J. Phys. Chem. Lett.* **2013**, *4*, 2069.

[65] R. C. I. Mackenzie, A. Göritz, S. Greedy, E. Von Hauff, J. Nelson, *Phys. Rev. B - Condens. Matter Mater. Phys.* **2014**, *89*, 195307.

[66] Z. Tang, Z. George, Z. Ma, J. Bergqvist, K. Tvingstedt, K. Vandewal, E. Wang, L. M. Andersson, M. R. Andersson, F. Zhang, O. Inganäs, *Adv. Energy Mater.* **2012**, *2*, 1467.

[67] W. F. Pasveer, J. Cottaar, C. Tanase, R. Coehoorn, P. A. Bobbert, P. W. M. Blom, M. De Leeuw, M. A. J. Michels, *Phys. Rev. Lett.* **2005**, *94*, 206601.

[68] V. I. Arkhipov, P. Heremans, H. Bässler, *Appl. Phys. Lett.* **2003**, *82*, 4605.

[69] B. A. Gregg, S. G. Chen, R. A. Cormier, *Chem. Mater.* **2004**, *16*, 4586.

[70] N. R. Monahan, K. W. Williams, B. Kumar, C. Nuckolls, X. Y. Zhu, *Phys. Rev. Lett.* **2015**, *114*, 247003.

[71] A. J. Barker, K. Chen, J. M. Hodgkiss, *J. Am. Chem. Soc.* **2014**, *136*, 12018.

[72] K. Chen, A. J. Barker, M. E. Reish, K. C. Gordon, J. M. Hodgkiss, *J. Am. Chem. Soc.* **2013**, *135*, 18502.

[73] B. Bernardo, D. Cheyns, B. Verreet, R. D. Schaller, B. P. Rand, N. C. Giebink, *Nat. Commun.* **2014**, *5*, 3245.

[74] U. Albrecht, H. Bässler, *Chem. Phys. Lett.* **1995**, *235*, 389.

[75] T. Offermans, S. C. J. Meskers, R. A. J. Janssen, *Chem. Phys.* **2005**, *308*, 125.

[76] S. N. Hood, I. Kassal, *J. Phys. Chem. Lett.* **2016**, *7*, 4495.

[77] J. Liu, S. Chen, D. Qian, B. Gautam, G. Yang, J. Zhao, J. Bergqvist, F. Zhang, W. Ma, H. Ade, O. Inganäs, K. Gundogdu, F. Gao, H. Yan, *Nat. Energy* **2016**, *1*, 16089.

[78] T. M. Burke, M. D. McGehee, *Adv. Mater.* **2014**, *26*, 1923.

[79] S. W. Kettlitz, J. Mescher, N. S. Christ, M. Nintz, S. Valouch, A. Colsmann, U.

Lemmer, *IEEE Photonics Technol. Lett.* **2013**, *25*, 682.

[80] C. Groves, *Energy Environ. Sci.* **2013**, *6*, 3202.

[81] A. Devižis, Charge Carrier Transport in Conjugated Polymer Films Revealed by Ultrafast Optical Probing, Vilnius University, **2011**.

[82] V. M. Le Corre, A. R. Chatri, N. Y. Doumon, L. J. A. Koster, *Adv. Energy Mater.* **2017**, *7*, 1701138.

[83] N. Felekidis, A. Melianas, L. Ever Aguirre, M. Kemerink, *Adv. Energy Mater.* **2018**, accepted.

[84] W. F. Pasveer, P. A. Bobbert, M. A. J. Michels, *Phys. Rev. B - Condens. Matter Mater. Phys.* **2006**, *74*, 165209.

[85] N. Vukmirović, C. S. Ponseca, H. Němec, A. Yartsev, V. Sundström, *J. Phys. Chem. C* **2012**, *116*, 19665.

[86] O. Hilt, L. D. A. Siebbeles, *Chem. Phys.* **1998**, *229*, 257.

[87] J. C. Blakesley, F. A. Castro, W. Kylberg, G. F. A. Dibb, C. Arantes, R. Valaski, M. Cremona, J. S. Kim, J. S. Kim, *Org. Electron. physics, Mater. Appl.* **2014**, *15*, 1263.

[88] S. Mukherjee, X. Jiao, H. Ade, *Adv. Energy Mater.* **2016**, *6*, 1600699.

[89] S. Mukherjee, C. M. Proctor, G. C. Bazan, T. Q. Nguyen, H. Ade, *Adv. Energy Mater.* **2015**, *5*, 1500877.

[90] B. A. Collins, Z. Li, J. R. Tumbleston, E. Gann, C. R. Mcneill, H. Ade, *Adv. Energy Mater.* **2013**, *3*, 65.

[91] J. Rivnay, S. C. B. Mannsfeld, C. E. Miller, A. Salleo, M. F. Toney, *Chem. Rev.* **2012**, *112*, 5488.

[92] C. M. Proctor, A. S. Kher, J. A. Love, Y. Huang, A. Sharenko, G. C. Bazan, T. Q. Nguyen, *Adv. Energy Mater.* **2016**, *6*, 1502285.

[93] S. Foster, F. Deledalle, A. Mitani, T. Kimura, K. B. Kim, T. Okachi, T. Kirchartz, J. Oguma, K. Miyake, J. R. Durrant, S. Doi, J. Nelson, *Adv. Energy Mater.* **2014**, *4*,

1400311.

[94] X. Guo, M. Zhang, J. Tan, S. Zhang, L. Huo, W. Hu, Y. Li, J. Hou, *Adv. Mater.* **2012**, *24*, 6536.

[95] K. Vandewal, S. Albrecht, E. T. Hoke, K. R. Graham, J. Widmer, J. D. Douglas, M. Schubert, W. R. Mateker, J. T. Bloking, G. F. Burkhard, A. Sellinger, J. M. J. Fréchet, A. Amassian, M. K. Riede, M. D. McGehee, D. Neher, A. Salleo, *Nat. Mater.* **2014**, *13*, 63.

[96] E. Frankevich, Y. Maruyama, H. Ogata, *Chem. Phys. Lett.* **1993**, *214*, 39.

[97] C. Lorch, K. Broch, V. Belova, G. Duva, A. Hinderhofer, A. Gerlach, M. Jankowski, F. Schreiber, *J. Appl. Crystallogr.* **2016**, *49*, 1266.

[98] M. Zhang, H. Wang, H. Tian, Y. Geng, C. W. Tang, *Adv. Mater.* **2011**, *23*, 4960.

[99] K. Vandewal, J. Widmer, T. Heumueller, C. J. Brabec, M. D. McGehee, K. Leo, M. Riede, A. Salleo, *Adv. Mater.* **2014**, *26*, 3839.

[100] D. Spoltore, A. Hofacker, J. Benduhn, S. Ullbrich, M. Nyman, O. Zeika, K. S. Schellhammer, Y. Fan, I. R. Ramirez, S. Barlow, M. Riede, S. R. Marder, F. Ortmann, K. Vandewal, *J. Phys. Chem. Lett.* **2018**, acs. jpclett.8b02177.

[101] F. Symalla, P. Friederich, A. Massé, V. Meded, R. Coehoorn, P. Bobbert, W. Wenzel, *Phys. Rev. Lett.* **2016**, *117*, DOI 10.1103/PhysRevLett.117.276803.

[102] S. M. Tuladhar, D. Poplavskyy, S. A. Choulis, J. R. Durrant, D. D. C. Bradley, J. Nelson, *Adv. Funct. Mater.* **2005**, *15*, 1171.

[103] A. Gadisa, K. Tvingstedt, K. Vandewal, F. Zhang, J. V. Manca, O. Inganäs, *Adv. Mater.* **2010**, *22*, 1008.

[104] R. H. Fowler, L. Nordheim, *Proc. R. Soc. A Math. Phys. Eng. Sci.* **1928**, *119*, 173.

[105] A. Massé, P. Friederich, F. Symalla, F. Liu, V. Meded, R. Coehoorn, W. Wenzel, P. A. Bobbert, *Phys. Rev. B* **2017**, *95*, 115204.

[106] U. Rau, *Phys. Rev. B - Condens. Matter Mater. Phys.* **2007**, *76*, DOI

10.1103/PhysRevB.76.085303.

[107] K. Vandewal, K. Tvingstedt, A. Gadisa, O. Inganäs, J. V. Manca, *Phys. Rev. B - Condens. Matter Mater. Phys.* **2010**, *81*, 125204.

[108] K. Vandewal, K. Tvingstedt, A. Gadisa, O. Inganäs, J. V. Manca, *Nat. Mater.* **2009**, *8*, 904.

[109] J. Kurpiers, D. Neher, *Sci. Rep.* **2016**, *6*, 26832.

[110] S. Roland, J. Kniepert, J. A. Love, V. Negi, F. Liu, P. Bobbert, M. Kemerink, A. Hofacker, D. Neher, *(Submitted manuscript) Adv. En. Mater.* **2018**.

[111] J. C. Blakesley, D. Neher, *Phys. Rev. B - Condens. Matter Mater. Phys.* **2011**, *84*, 075210.

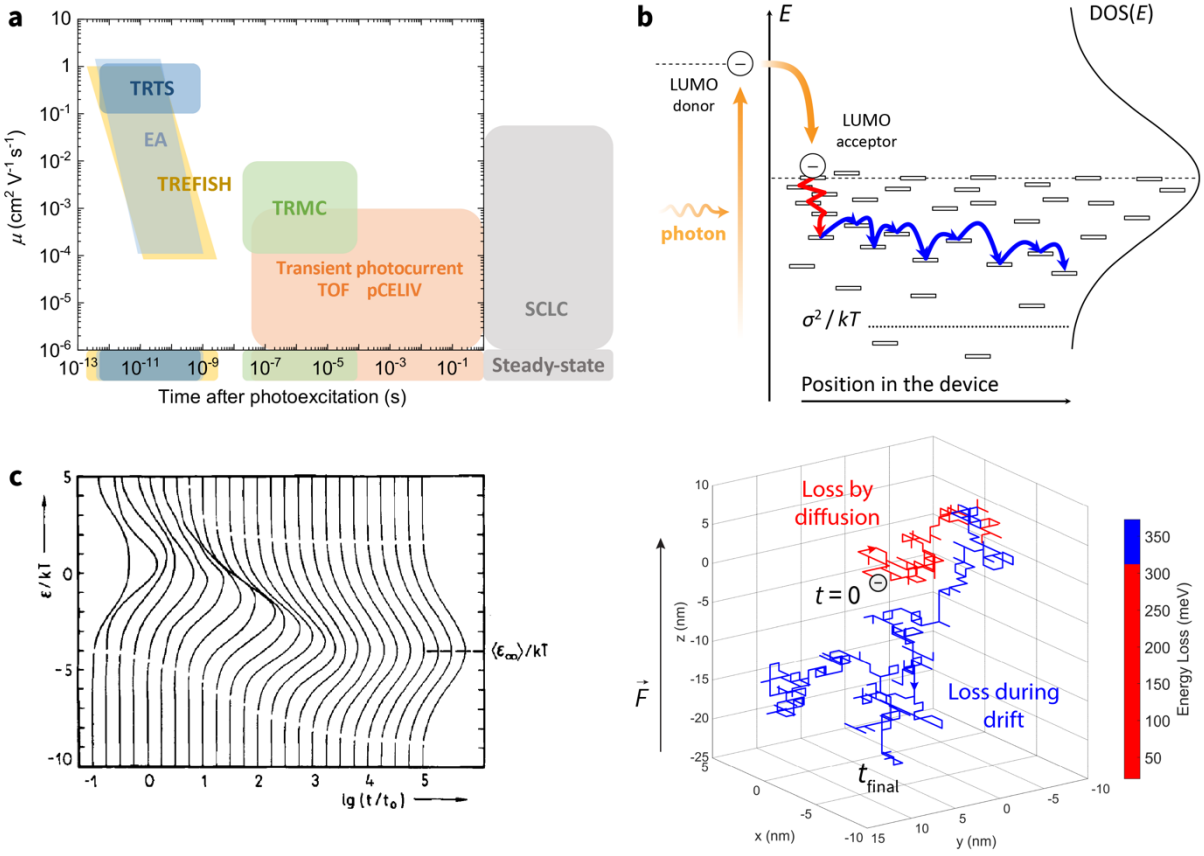

Figure 1. Non-equilibrium motion of photogenerated charges. (**a**) Typical charge carrier mobility values in OPV, obtained by the various experimental techniques. The indicated values are a guide to the eye and not a fully exact representation of the literature data. (**b**) Top: Schematic description of photoinduced electron transfer (orange arrows) followed by photogenerated carrier thermalization in an OPV device. First, most of the excess energy (1-2σ) is lost by fast diffusive motion, as indicated by the red hopping arrow going back and forth. At later time scales, the drift component of motion gradually becomes more important and directed transport to the extracting electrode begins (blue arrows). During transport to the electrode, the remainder of the excess energy is continuously, but not entirely, lost to further thermalization.[21] Bottom: Corresponding simulated spatially-resolved motion of a photogenerated electron in TQ1:$PC_{71}BM$ (1:2.5), initially positioned at [0 0 0]. The electric field F (0.2V / 100nm, corresponding to MPP conditions) is driving the electron downwards (to negative z values), but has little effect at early time scales (<1 ns in this case). Most of the excess photon energy is lost by fast diffusion-dominated motion (red), followed by a slower and smaller loss during drift-dominated extraction (blue). The color bar shows only two colors for clarity. Adapted with permission.[21,23] (**c**) Photogenerated carrier thermalization in a disordered organic semiconductor, according to the Gaussian Disorder Model (GDM) developed by Bässler et al. Reproduced with permission.[24] 2013, Copyright Wiley-VCH Verlag GmbH & Co. KGaA.

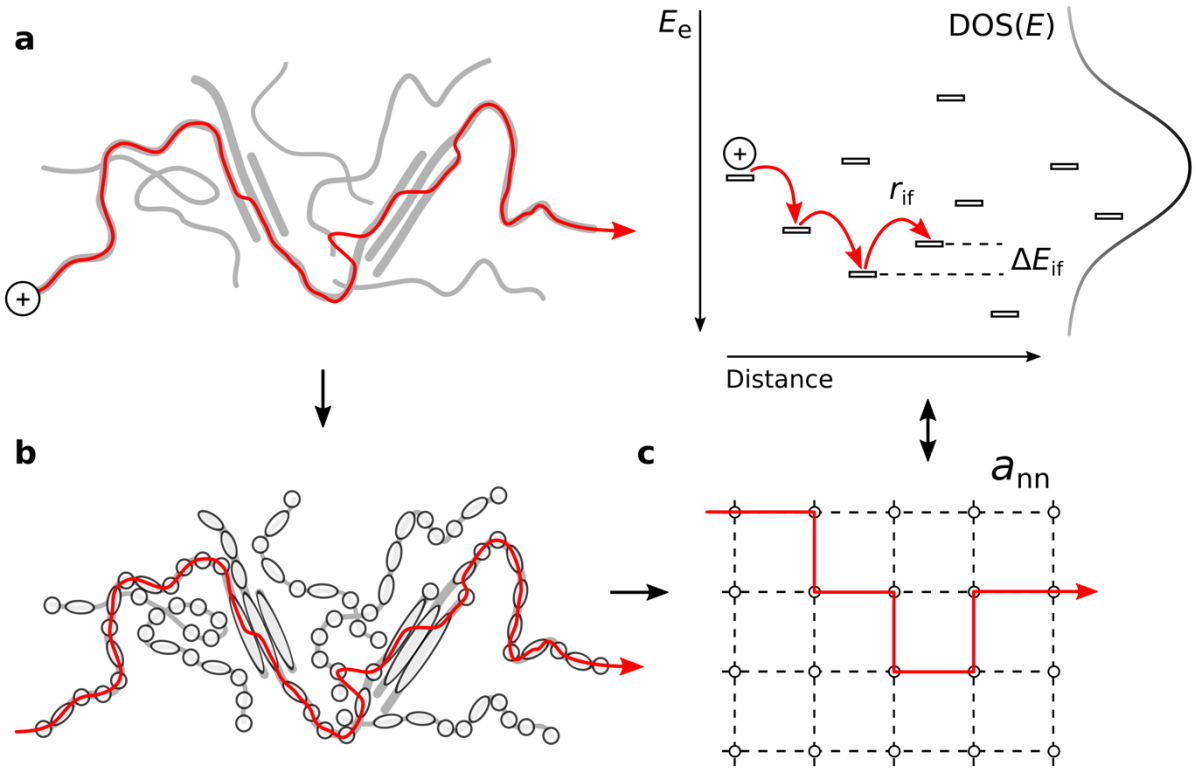

Figure 2. Schematic description of the Gaussian Disorder Model (GDM). The polymer chains in (**a**) are subdivided into conjugated units or hopping sites, shown in (**b**), via which charge transport (red arrow) takes place. (**c**) The GDM model represents the electronic sites as a grid, where the site energies are drawn from a Gaussian distribution according to Equation (2). The energy axis in the top right Figure corresponds to electron energy (E_e), hole hopping in this case occurs from top to bottom. Adapted with permission.[23]

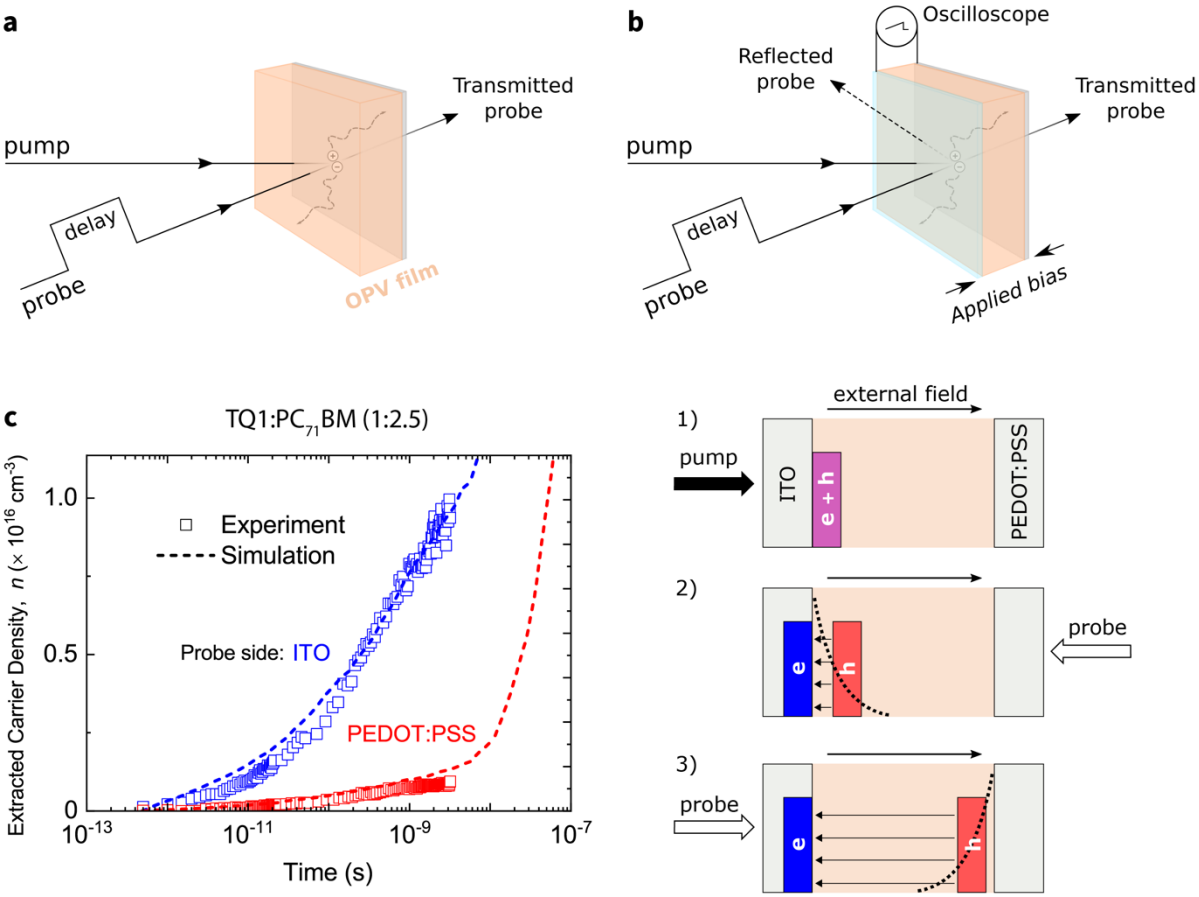

Figure 3. Schematic description of time-resolved experiments. Transient measurements are typically performed either on thin films (**a**) or complete solar cell devices with electrodes (**b**). If a metallic back electrode is used, the probe is reflected (dashed arrow), whereas for semi-transparent devices, the probe is transmitted (solid arrow). (**c**) TREFISH experiment on an optically thick TQ1:$PC_{71}BM$ (1:2.5) device (see section 5.1). The right-side shows the measurement schematic: (1) The pump creates a relatively narrow distribution of photogenerated charges (purple rectangle). (2) Only when the region where the electric field is present, i.e. between the sheets of electrons (blue) an holes (red), extends to the area "seen" by the probe (dotted lines) a TREFISH signal is measured. The probed area is on the opposite side of the sample with respect to the incident pump. This is because the second harmonic is reabsorbed by the active layer and only the indicated fraction (dotted lines) can exit the device for detection. Since holes drift much slower than electrons and need to traverse a larger distance, the TREFISH signal at the ITO electrode is seen at short times (2), whereas the signal at the PEDOT:PSS electrode is delayed (3). Left-side shows that the measurement results are in good agreement with 3D kMC simulations. Adapted with permission.[19,23] 2014, Copyright Wiley-VCH Verlag GmbH & Co. KGaA.

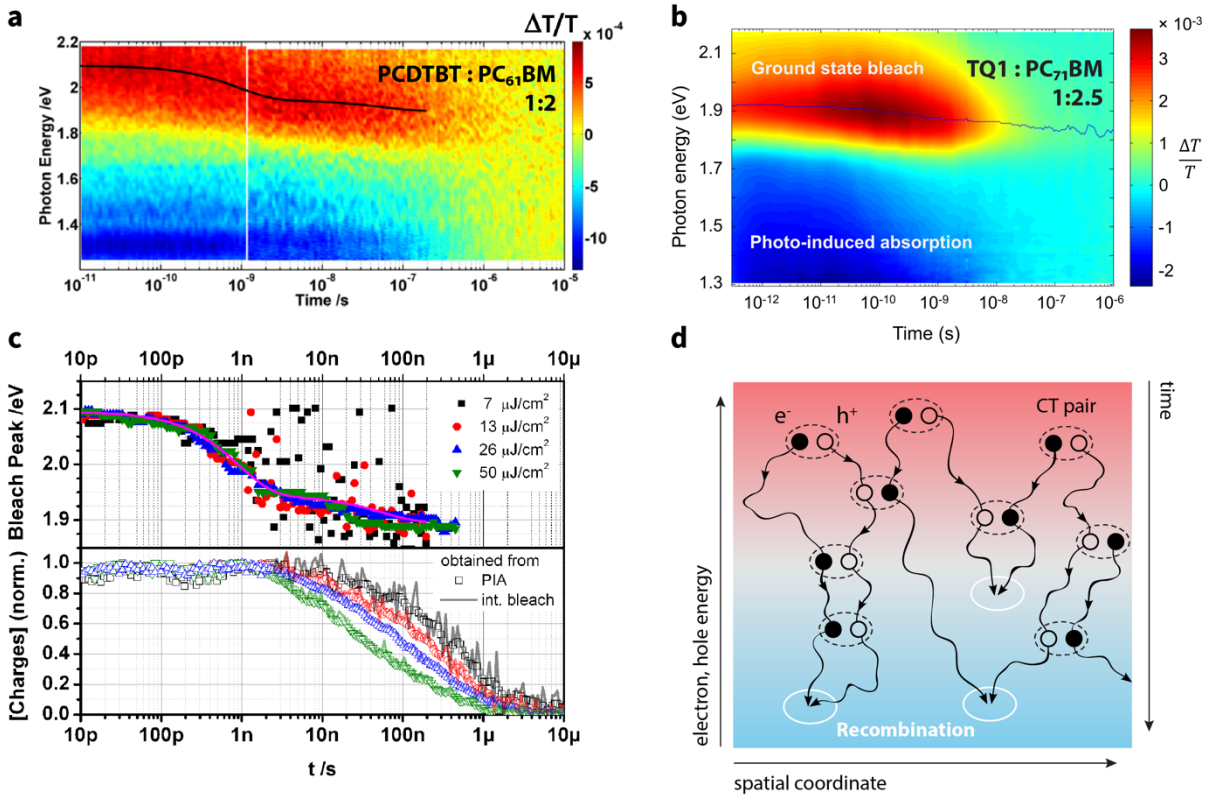

Figure 4. Non-equilibrium photogenerated carrier dynamics as revealed by Transient Absorption (TA) spectroscopy. TA dynamics of TQ1:$PC_{71}BM$ (1:2.5) (**a**) and PCDTBT:$PC_{61}BM$ (1:2) (**b**), the redshift of the GSB peak maximum is highlighted by the solid black trace. (**c**) Top: GSB redshift dynamics confirm that photogenerated carrier thermalization is pump-fluence independent. Bottom: comparison of integrated GSB and PIA dynamics confirms that the GSB redshift and PIA originate from the same charge carrier population (hole polarons). (**d**) Schematic illustrating photogenerated carrier recombination/thermalization in their respective disorder broadened DOS (shaded background). Dashed circles indicate the temporary presence of a charge transfer (CT) pair, white circles indicate CT recombination. Adapted with permission.[21,23,45] 2014, Copyright Wiley-VCH Verlag GmbH & Co. KGaA.

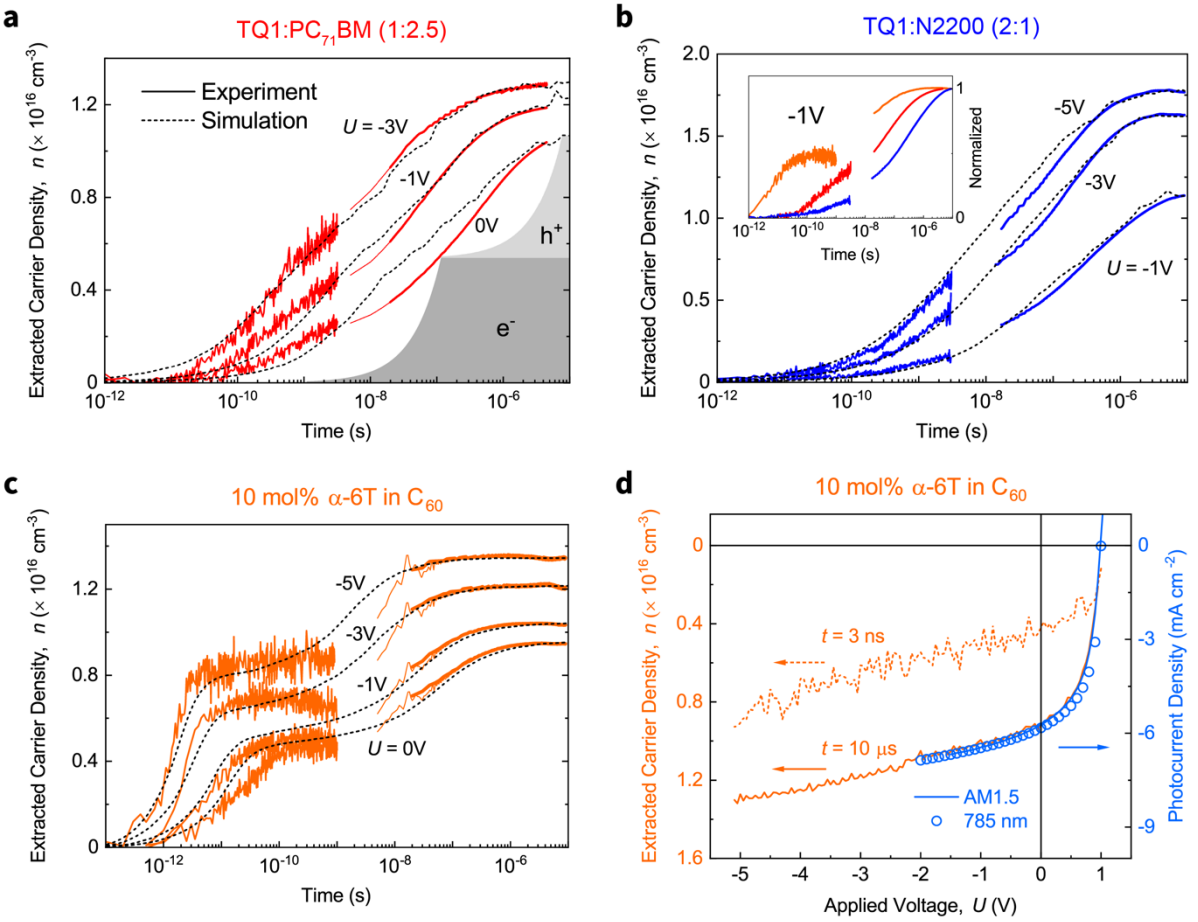

Figure 5. Time-resolved charge extraction measured by TREFISH and transient photocurrent. In panels a-c the colored traces mark experiments, whereas the black dashed traces are simulations. (**a**) TQ1:$PC_{71}BM$ (1:2.5). The shaded areas illustrate extraction in case of non-dispersive transport and quasi-equilibrium mobilities (**b**) TQ1:N2200 (2:1). (**c**) α-6T:C_{60} (10 mol% α-6T). The inset in panel b compares charge extraction in these blends. (**d**) Comparison of extracted charge at 3 ns (dashed traces) and full extraction (solid traces) as measured by TREFISH and transient photocurrent on α-6T:C_{60} in panel c. The blue traces correspond to the photocurrent-voltage curves measured under steady-state AM1.5 illumination (solid blue) and continuous 785 nm laser illumination (open blue circles), highlighting the relevance of these time-resolved experiments to steady-state OPV device operation. Adapted with permission.[20,22] 2017, Copyright Wiley-VCH Verlag GmbH & Co. KGaA.

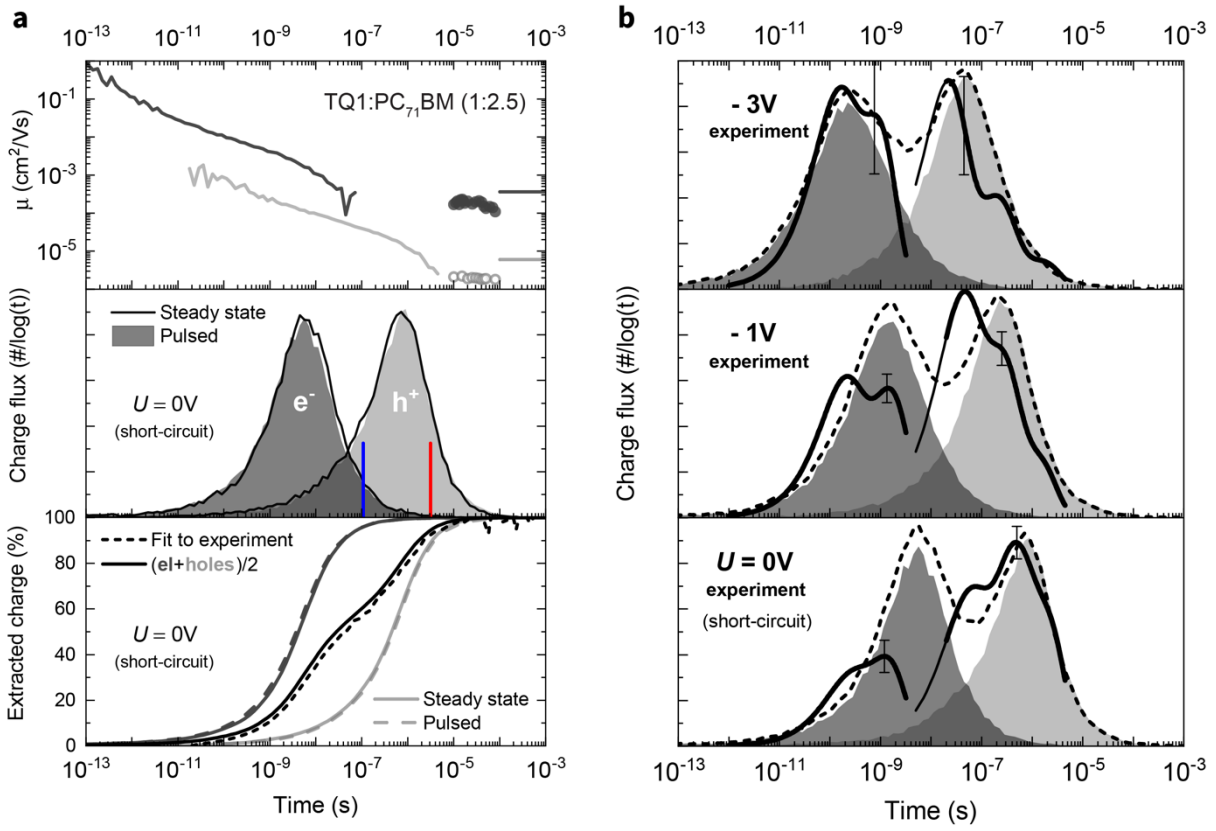

Figure 6. Time-dependent mobility and dispersion in charge extraction times. Data for TQ1:$PC_{71}BM$ (1:2.5). (**a**) Top: time-dependent mobility used to fit the experimental TREFISH and transient photocurrent measurements in Figure 5a. Middle: Simulated charge extraction histograms under pulsed and steady-state illumination are identical, highlighting the relevance of these results to steady-state device operation. The colored vertical bars mark the mean extraction times for the holes (red) and electrons (blue) which are a poor description of the actual charge extraction histograms. Bottom: Integrated charge extraction histograms shown in the middle panel. (**b**) Bias-dependent charge extraction histograms. Shaded areas are simulated electron (darker shade) and hole (lighter shade) extraction at the indicated applied bias, whereas the black dashed trace is their sum. The thick solid traces are experimentally determined charge extraction histograms from the experimental data in Figure 5a. Adapted with permission.[19] 2014, Copyright Wiley-VCH Verlag GmbH & Co. KGaA.

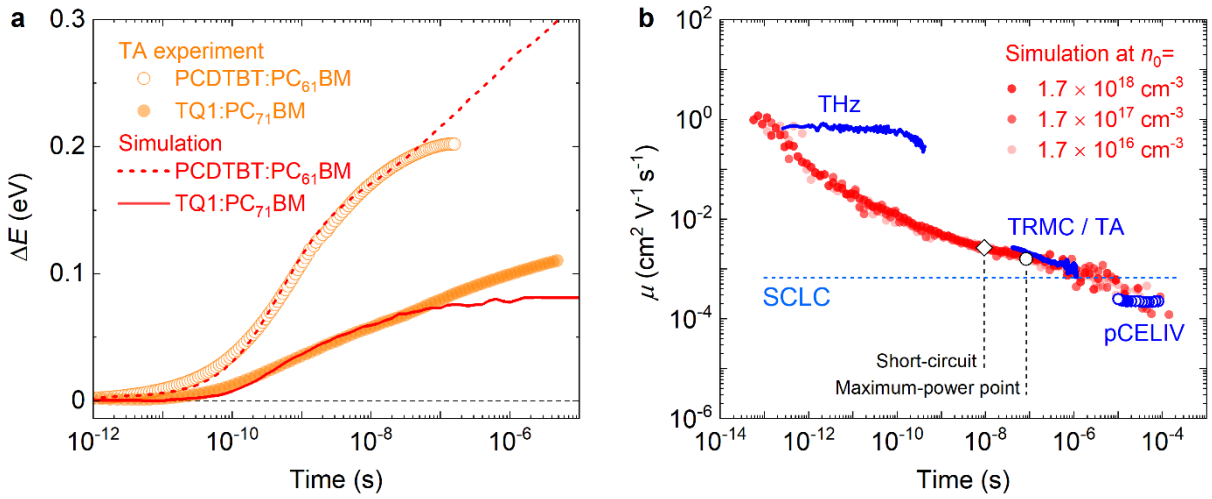

Figure 7. Photogenerated carrier thermalization and time-dependent carrier mobility. (**a**) Time-resolved GSB redshift ΔE for TQ1:$PC_{71}BM$ 1:2.5 (filled circles) and PCDTBT:$PC_{61}BM$ 1:2 (open circles) and the corresponding 3D kMC simulations (red traces). Experimental data correspond to Figs. 4a-b. (**b**) Time-dependent carrier mobility in TQ1:$PC_{71}BM$ measured by the indicated experimental technique (blue traces) is in good agreement with 3D kMC simulations (red symbols). The time-dependent mobility is independent of initial carrier density, highlighting the absence of state-filling effects due to the non-equilibrium nature of carrier thermalization. The blue dashed line marks a representative SCLC mobility measured in the dark (see section 6). Note the similarity to Figure 1a. Extraction times at short-circuit (black empty diamond) and at maximum-power point (black empty circle) mark the relevant time scales for electron extraction in a 70 nm thick TQ1:$PC_{71}BM$ (1:2.5) device. Adapted with permission.[21,23]

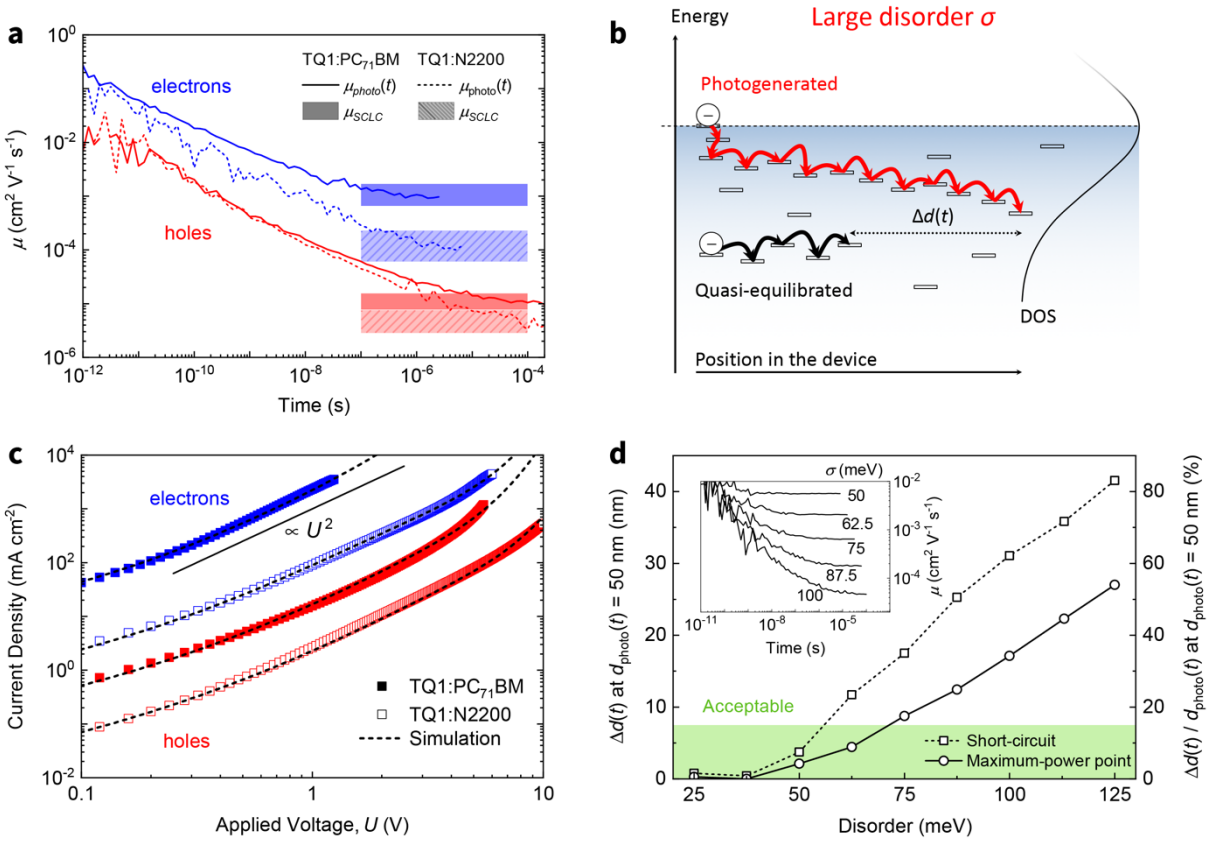

Figure 8. Comparison of photogenerated and SCLC carrier mobility in TQ1:$PC_{71}BM$ (1:2.5) and TQ1:N2200 (2:1). (**a**) Comparison of the time-dependent photogenerated carrier mobility to that of carriers injected from the electrodes in the dark, as determined by SCLC (shaded areas). (**b**) In materials with large energetic disorder, the photogenerated carriers drift significantly larger distances than quasi-equilibrated carriers within the same time period – the latter are lagging behind by $\Delta d(t)$. (**c**) IV characteristics of hole- and electron-only SCLC diodes measured in the dark. (**d**) Predicted error for a hypothetical material with the indicated disorder. The error is calculated at short-circuit (1V / 100nm) and maximum-power point (0.2V / 100nm) conditions at a photogenerated carrier drift distance of $d_{photo}(t)$ = 50 nm. The inset shows that the photogenerated carrier mobility becomes less time-dependent with decreasing disorder, reducing the error. The green shaded area marks the suggested acceptable error. Adapted with permission.[20,23] 2017, Copyright Wiley-VCH Verlag GmbH & Co. KGaA.

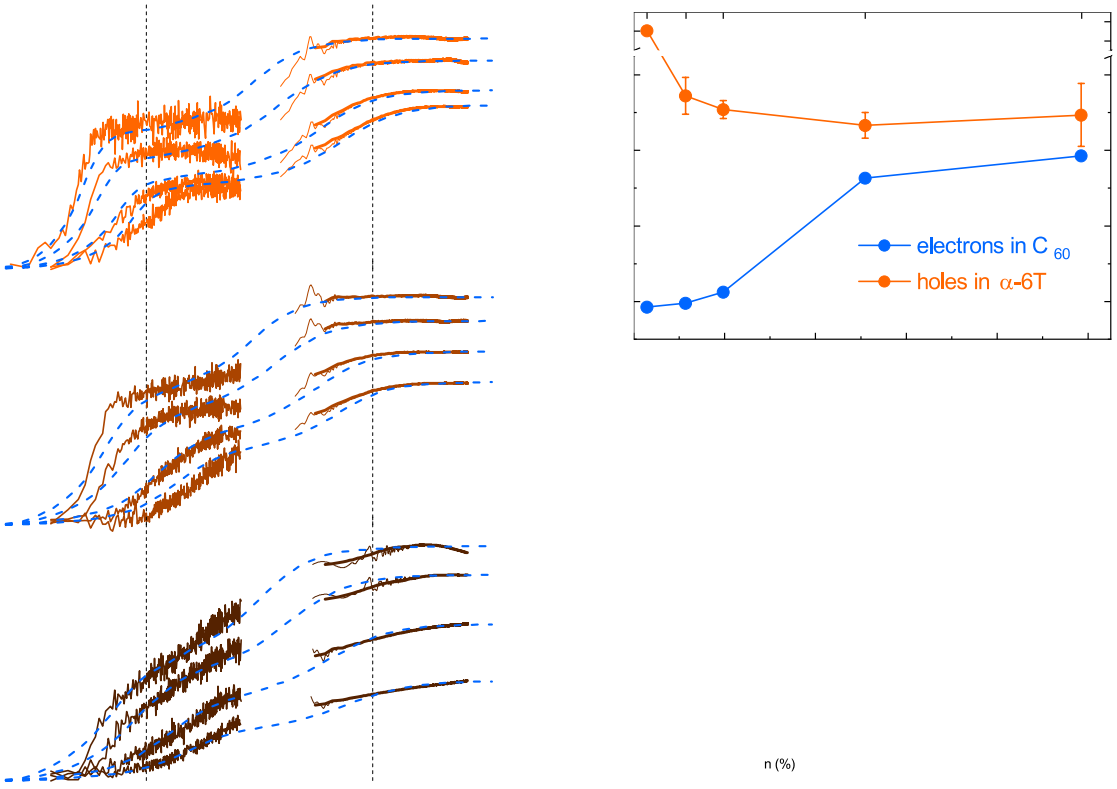

Figure 9. Effects of phase purity on charge transport. (**a**) Time-resolved charge extraction experiments at the indicated applied bias (orange traces), fitted by a model incorporating the GDM framework (blue dashed traces) involving three charge populations: electrons in C_{60}, holes in C_{60} and holes tunneling through C_{60} between isolated α-6T sites, see section 7.2. Measurements were performed using CT photoexcitation.[22] (**b**) Electron (blue) and hole (orange) energetic disorder versus α-6T content. (**c**) Time-dependent mobility of photogenerated electrons (blue) and holes (orange). The inset shows complementary SCLC measurements, showing the same trends as in the transient measurements. The increase in the SCLC mobility at 1.5 mol% donor marks the onset for efficient long-range hole tunneling, see section 7.2. Adapted with permission.[20,23] 2017, Copyright Wiley-VCH Verlag GmbH & Co. KGaA.

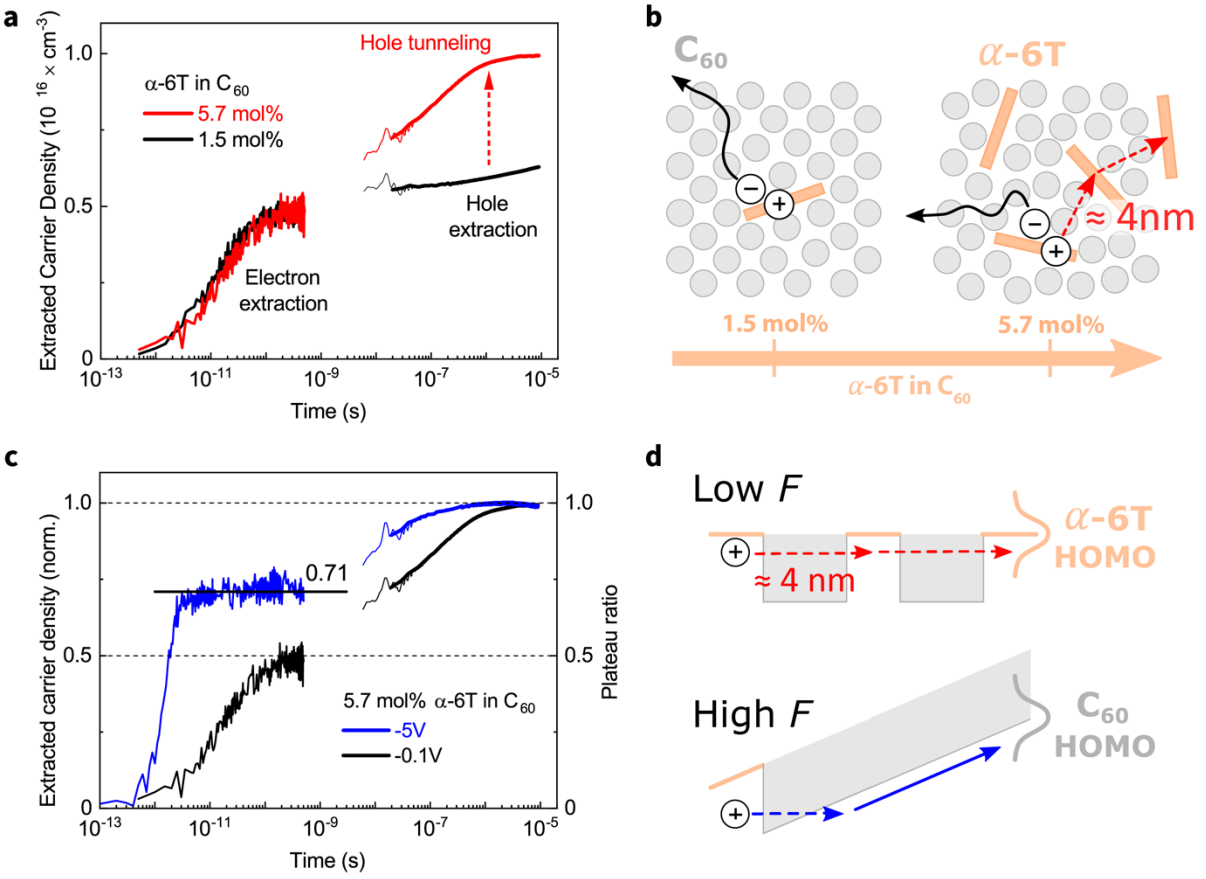

Figure 10. Long-range hole tunneling between non-nearest-neighbor donor molecules and hole extraction via C_{60}. (**a**) Combined TREFISH and transient photocurrent measurements reveal an onset for long-range hole tunneling (red dashed arrows in panel (**b**) schematic) at an average inter-donor site distance of ~4 nm. (**c**) Normalized transient extraction kinetics show the increasing contribution of the first extraction plateau with increasing reverse bias. (**d**) Schematic representation of the two mechanisms for hole transport in α-6T:C_{60}. Black dashed arrows indicate long-range hole tunneling through C_{60} to nearby α-6T sites, whereas red dashed arrows indicate hole de-trapping from α-6T to C_{60} by Fowler-Nordheim type tunneling (possible only at very high electric fields F). Adapted with permission.[23]

Author Biographies

Armantas Melianas is currently a Wallenberg Foundation postdoctoral scholar at Stanford University. He received his Ph.D. in Applied Physics from Linköping University (2017) on time-resolved charge transport in organic photovoltaic devices. His current research interests include the physics of organic electronic materials and devices and their use in applications ranging from energy harvesting to brain-inspired (neuromorphic) computing.

Martijn Kemerink is a group leader and full professor in Applied Physics at Linköping University since 2014. He obtained a PhD in Applied Physics from Eindhoven University of Technology (1998) on many body effects in III/V semiconductor heterostructures. Later, he shifted his research focus towards scanning probe microscopy and organic electronics. His current research focuses on the physics of organic materials and devices for energy harvesting and memory applications.

Table of Contents Summary:

Unification of time-resolved and steady-state techniques probing photogenerated charge motion in organic electronic materials is presented. Charge separation, recombination and transport in organic solar cells are experimentally shown to be governed by non-equilibrium motion of photogenerated carriers, driven by slow thermalization. Kinetic Monte Carlo modelling unifies these observations in a single framework and highlights their importance when describing operating devices.

Keywords: thermalization, organic solar cells, kinetic Monte Carlo simulations, charge carrier mobility, non-equilibrium phenomena

Authors: Armantas Melianas*, Martijn Kemerink*

Title: Photogenerated Charge Transport in Organic Electronic Materials: Experiments Confirmed by Simulations

Table of Contents Figure: